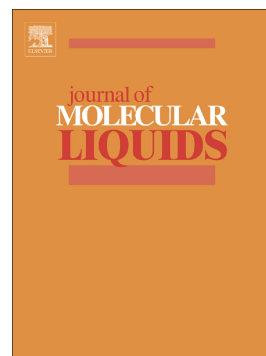


## Accepted Manuscript

Amino acid based imidazolium zwitterions as novel and green corrosion inhibitors for mild steel: Experimental, DFT and MD studies

V. Srivastava, Jiyaul Haque, C. Verma, P. Singh, H. Lgaz, R. Salghi, M.A. Quraishi



PII: S0167-7322(17)31227-8  
DOI: doi: [10.1016/j.molliq.2017.08.049](https://doi.org/10.1016/j.molliq.2017.08.049)  
Reference: MOLLIQ 7757

To appear in: *Journal of Molecular Liquids*

Received date: 21 March 2017  
Revised date: 5 August 2017  
Accepted date: 12 August 2017

Please cite this article as: V. Srivastava, Jiyaul Haque, C. Verma, P. Singh, H. Lgaz, R. Salghi, M.A. Quraishi , Amino acid based imidazolium zwitterions as novel and green corrosion inhibitors for mild steel: Experimental, DFT and MD studies, *Journal of Molecular Liquids* (2017), doi: [10.1016/j.molliq.2017.08.049](https://doi.org/10.1016/j.molliq.2017.08.049)

This is a PDF file of an unedited manuscript that has been accepted for publication. As a service to our customers we are providing this early version of the manuscript. The manuscript will undergo copyediting, typesetting, and review of the resulting proof before it is published in its final form. Please note that during the production process errors may be discovered which could affect the content, and all legal disclaimers that apply to the journal pertain.

## Amino acid Based Imidazolium Zwitterions as Novel and Green Corrosion Inhibitors for Mild Steel: Experimental, DFT and MD Studies

V. Srivastava<sup>1</sup>, Jiyaul Haque<sup>1</sup>, C. Verma<sup>1,3</sup>, P. Singh<sup>1</sup>, H. Lgaz<sup>4,5</sup>, R. Salghi<sup>4</sup>, M.A. Quraishi<sup>1,2,\*</sup>

<sup>1</sup>*Department of Chemistry, Indian Institute of Technology (Banaras Hindu University), Varanasi -221005, India.*

<sup>2</sup>*Center of Research Excellence in Corrosion, Research Institute, King Fahd University of Petroleum and Minerals, Dhahran 31261, Saudi Arabia.*

<sup>3</sup>*Material Science Innovation and Modelling (MaSIM) Research Focus Area, Department of Chemistry, Faculty of Agriculture, Science and Technology, North-West University (Mafikeng Campus), Private Bag X2046, Mmabatho 2735, South Africa*

<sup>4</sup>*Laboratory of Applied Chemistry and Environment, ENSA, Universite Ibn Zohr, PO Box 1136, 80000 Agadir, Morocco.*

<sup>5</sup>*Laboratory of separation methods, Faculty of Science, Ibn Tofail University PO Box 242, Kenitra, Morocco,*

\*Corresponding author:

Ph.no. +91-9307025126

E-mail: maquraishi.apc@itbhu.ac.in

### Abstract

Three novel amino acids based corrosion inhibitors namely 2-(3-(carboxymethyl)-1H-imidazol-3-ium-1-yl)acetate (AIZ-1), 2-(3-(1-carboxyethyl)-1H-imidazol-3-ium-1-yl)propanoate (AIZ-2) and 2-(3-(1-carboxy-2-phenylethyl)-1H-imidazol-3-ium-1-yl)-3-phenylpropanoate (AIZ-3) were synthesized by condensing glyoxal, formaldehyde and amino acids, and characterized. The corrosion inhibition performance of synthesized inhibitors was studied by electrochemical impedance (EIS) and potentiodynamic polarization (PDP) methods. Among the studied inhibitors, AIZ-3 showed the maximum inhibition efficiency (IE) of 96.08% at a concentration as low as 0.55 mM (200 ppm). The results of potentiodynamic study reveal that AIZ-1 acts as cathodic inhibitor while AIZ-2 and AIZ-3 act as mixed type inhibitors. The results of EIS studies showed that in the presence of inhibitors, polarization resistance increased and  $C_{dl}$

decreased due adsorption of inhibitors at the metal surface. The adsorption of AIZs on the mild steel surface followed the Langmuir adsorption isotherm. The result of scanning electron microscope (SEM), atomic force microscope (AFM) and energy-dispersive X-ray spectroscopy (EDX) supported the formation of inhibitors film on the metal surface. The quantum chemical parameters and molecular dynamics (MD) simulations were used to study the reactivity and adsorption behavior of zwitterions. The results of the theoretical investigation and experimental studies well complimented each other.

*Keywords:* Mild Steel, Corrosion inhibition, Quantum chemical calculation, MD, imidazolium zwitterions.

## 1. Introduction

Each country loses 3-5% of its GDP on account of corrosion. The global economic loss due to corrosion is approximately \$2.5 trillion estimated by National Association of Corrosion Engineers (NACE) in 2016 [1]. Mild steel finds wide applications in various industries, because of its low cost and excellent mechanical strength. However, it undergoes severe corrosion when it is exposed to the acid solution during pickling and acid cleaning, descaling and oil-well acidification [2, 3]. Inhibitors are added to acid solutions to prevent metal dissolution. The use of inhibitors is one of the most practical methods to protect metals from corrosion. Most of the synthetic inhibitors are toxic and cause health hazards [4]. Therefore, their replacement by the environmentally benign inhibitors is desirable. Amino acids have been reported as effective corrosion inhibitors [5-8]. They are naturally occurring chemicals, biodegradable and show the wide range of pharmaceutical and biological activities [9, 10].

It is well documented in the literature that amino acids exhibit relatively low IE at the higher concentration when they are used alone. Sorkhabi *et al.* [11] found that alanine and glycine exhibit the maximum IE of 80% and 78.9%, respectively for steel corrosion in 0.1M HCl at 10 mM. Amin *et al.* [12] tested alanine, s-methyl cysteine and cysteine as corrosion inhibitors on iron in 1 M HCl solution. These compounds gave maximum inhibition efficiencies of 77.3%, 86% and 94.2%, respectively at 5.0 mM. Mobin *et al.* and Zhang *et al.* have studied the synergistic effect of halides and surfactants for the improvement of inhibition efficiency of

amino acids, but they did not find significant enhancement of inhibition efficiency [13-14]. In our previous study, we have synthesized a condensation product of histidine and cysteine and investigated its corrosion inhibition effect on mild steel in 1 M HCl. It gave the better inhibition as compared to individual amino acids [15]. In view of the high performance of the condensation product histidine and cysteine, we have synthesized three condensation products namely 2-(3-(carboxymethyl)-1H-imidazol-3-ium-1-yl)acetate (AIZ-1), 2-(3-(1-carboxyethyl)-1H-imidazol-3-ium-1-yl)propanoate (AIZ-2) and 2-(3-(1-carboxy-2-phenylethyl)-1H-imidazol-3-ium-1-yl)-3-phenylpropanoate (AIZ-3) and evaluated them as corrosion inhibitors for mild steel in 1 M HCl. The selection of these inhibitors is based on the facts that they are nontoxic, conveniently synthesized in good yield and are soluble in aqueous acid solution. In addition to this, the chemical structure of selected inhibitors (Fig. 1) consist of one imidazole ring and two carboxylate groups, through which, they can adsorb on mild steel surface and are likely to give effective corrosion inhibition. The corrosion inhibition effect of above three inhibitors has been studied by electrochemical impedance spectroscopy (EIS), potentiodynamic polarization and gravimetric methods. The atomic force microscopy (AFM), scanning electron microscopy (SEM) and energy dispersive X-ray spectroscopy (EDX) were used for surface analyses. The quantum chemical method and MD methods were also used to correlate the theoretical and experimental results. The survey of literature reveals that these compounds have not been tested as corrosion inhibitors.

## 2. Experimental procedure

### 2.1. Synthesis of corrosion inhibitors (AIZs)

The investigated inhibitors were synthesized by the previously reported method [16]. The scheme of inhibitors synthesis is shown in Fig.1. The synthesized compounds were characterized by their FT-IR and  $^1\text{H}/^{13}\text{C}$  NMR techniques. The IR spectra were recorded using an FT-IR (Perkin Elmer, Bruker) spectrophotometer and  $^1\text{H}/^{13}\text{C}$  NMR spectra were recorded on a Bruker instrument at 500 MHz, respectively. The characterization data of the synthesized compounds are given in Table 1 and their corresponding FT-IR and  $^1\text{H}/^{13}\text{C}$  NMR spectra are shown in Figs. S1 and S2.

## 2.1. Materials and test solution

The mild steel specimens having chemical composition (wt %) C 0.076%, Si 0.026%, Mn 0.192, P 0.012%, Cr 0.050%, Ni 0.050%, Al 0.023% and Cu 0.135% and Fe 99.30% were used for gravimetric and electrochemical experiments. The specimens with dimension 2.5 cm × 2.0 cm × 0.025 cm were used for gravimetric test. The mild steel specimens were abraded by SiC abrasive papers (from grade 600 to 1200), rinsed with distilled water, degreased in acetone and dried in hot air and stored in moisture free desiccators before their use [17]. The test solution of 1M HCl was prepared by the dilution of analytical grade hydrochloric acid (HCl, 37 %, Fisher Scientific) with double distilled water.

## 2.2 Corrosion tests

### 2.2.1 Gravimetric measurement

Gravimetric experiments were carried out at different temperature (308-338K) as described in our earlier work [15]. The previously weighed mild steel specimens were immersed in 100 ml of 1M HCl without and with different concentrations of AIZs inhibitors for 3 hours. After immersion time, the sample was taken out, washed, dried and weighed again in order to calculate the weight loss. Each experiment was repeated twice and mean value was reported in order to achieve reproducibility of the results. The corrosion rate ( $C_R$ ), inhibition efficiency (IE %) and surface coverage ( $\theta$ ) can be calculated by using the following equations:

$$C_R = \frac{w}{At} \quad (1)$$

$$IE(\%) = \frac{C_R - C_{R(i)}}{C_R} \times 100 \quad (2)$$

$$\theta = \frac{C_R - C_{R(i)}}{C_R} \quad (3)$$

where  $w$ ,  $A$  and  $t$  are the weight loss (mg), the area of the specimen (cm<sup>2</sup>) and exposure time ( $h$ ) respectively.  $C_R$  and  $C_{R(i)}$  are the corrosion rate in absence and presence of AIZ molecules.

### 2.2.2 Electrochemical test

The electrochemical tests were carried out to corroborate the results of gravimetric measurement. A conventional three-electrode glass cell consisting of mild steel specimen with the 1cm<sup>2</sup> (one-sided) exposure area was used as working electrode (WE), platinum foil counter electrode (CE) and saturated calomel reference electrode (RE) were used for all the electrochemical experiments. All the electrochemical experiments were performed by using the Gamry Potentiostat/Galvanostat (Model G-300) instrument and Gamry Echem Analyst 5.0 software was used for fitting and analyzing the electrochemical data. EIS and PDP experiments were carried out at room temperature (35 ± 1 °C) in the unstirred solution. The electrochemical experiments were carried out after 30 min immersion time to stabilize the corrosion potential of mild steel.

The EIS experiment was carried out in the frequency range 100 kHz to 0.01 Hz with a sinusoidal amplitude of 10 mV AC signal. Polarization resistance ( $R_p$ ), double layer capacitances ( $C_{dl}$ ) and other parameters were calculated by the fitting Nyquist plot. The inhibition efficiency was calculated by applying the following equation:

$$IE(\%) = \frac{R_p^i - R_p^0}{R_p^i} \times 10 \quad (4)$$

where  $R_p^0$  and  $R_p^i$  are the polarization resistances in the absence and presence of different concentrations of AIZ molecules, respectively. Potentiodynamic polarization experiment was performed after 30 min at a constant sweep rate of 1 mV/s in the potential range from ± 0.25 V vs open circuit potential (OCP). Electrochemical parameters such as corrosion current density ( $i_{corr}$ ), corrosion potential ( $E_{corr}$ ) and cathodic ( $\beta_c$ ) and anodic ( $\beta_a$ ) Tafel slopes were derived by the extrapolation. The inhibition efficiency was calculated using following equation:

$$IE(\%) = \frac{i_{corr}^0 - i_{corr}^i}{i_{corr}^0} \times 100 \quad (5)$$

where the  $i_{corr}^0$  and  $i_{corr}^i$  are the corrosion current density in the absence and presence of AIZ molecules.

### 2.2.3 Surface analysis (AFM, SEM and EDX)

For the surface studies, mild steel specimens were prepared according to the previously reported method [18]. The surface morphological studies were carried out on mild steel samples after immersing in absence and presence of optimum concentration of AIZs. Scanning electron microscope (SEM-EDX), Zeiss Evo 50 XVP was used to study the changes occurring on metal surface along with the elemental composition. The SEM images were taken at 500x magnification. AFM technique was used to calculate the surface roughness for mild steel samples immersed without and with AIZs. Atomic force microscopy, NT-MDT multimode AFM, Russia, 111, was used to capture the micrographs.

### 2.2.4 Quantum chemical calculation

Quantum chemical calculations were performed by using Gaussian 09 suited program [19]. The complete geometry optimization was conducted by the DFT with Becke's three parameter exchange functional with the Lee–Yang–Paar correlation functional (B3LYP) [20]. The calculation was carried out by using the basis set 6-311G(d,p) for protonated forms. The self-consistent reaction field (SCRF) theory, with Tomasi's polarized continuum model (PCM) was applied to perform the computations in solution. The quantum chemical parameters such as the energy of the highest occupied molecular orbital ( $E_{HOMO}$ ) and that of the lowest unoccupied molecular orbital ( $E_{LUMO}$ ) have been calculated by optimized molecular structures of AIZs. Other quantum chemical parameters such as energy gap ( $\Delta E$ ), hardness ( $\eta$ ), softness ( $\sigma$ ), electronegativity ( $\chi$ ) and the fraction of electrons transferred ( $\Delta N$ ) were calculated by using the following equations:

$$\Delta E = E_{LUMO} - E_{HOMO} \quad (6)$$

$$\eta = \frac{1}{2}(E_{LUMO} - E_{HOMO}) \quad (7)$$

$$\chi = -\frac{1}{2}(E_{LUMO} + E_{HOMO}) \quad (8)$$

$$\Delta N = \frac{\chi_{Fe} - \chi_{inh}}{2(\eta_{Fe} + \eta_{inh})} = \frac{\phi - \chi_{inh}}{2(\eta_{Fe} - \eta_{inh})} \quad (9)$$

In equation (9), the electronegativity of iron metal surface  $\chi_{\text{Fe}}$  is replaced by the work function ( $\phi$ ), previously described [18, 21]. The  $\phi$  values obtained from DFT calculation are 3.91, 4.82 and 3.88 eV for the Fe (100), Fe (110) and Fe (111), respectively. Herein, we have chosen Fe (110) surface due to its high stabilization energy and packed structure.

Parr et al. [22] introduced electrophilicity index ( $\omega$ ) (Eq. 11), which is the inverse of the nucleophilicity. The electrophilicity of a chemical compound is associated with its electronegativity and hardness. The equations are shown as:

$$\varepsilon = \frac{1}{\omega} \quad (10)$$

$$\omega = \frac{\mu^2}{4\eta} = \frac{\chi^2}{4\eta} \quad (11)$$

### 2.2.5 Molecular dynamic details

MD simulations for investigated AIZ molecules were carried out in a simulation box with periodic boundary conditions using Materials Studio 6.0 (from Accelrys Inc.) [23]. The iron crystal was imported and cleaved along (110) plane and a slab of 5 Å was employed. The Fe (110) surface was relaxed by minimizing its energy using smart minimizer method. Fe (110) surface was enlarged to a (10 × 10) supercell to provide a large surface for the interaction of the inhibitors. A vacuum slab with zero thickness was built. In 1 M HCl, the corresponding proportion of water molecules to hydrogen chloride was 500/9, based on this, a supercell with a size of a = b = 24.82 Å c = 25.14 Å, contains 491 H<sub>2</sub>O, 9Cl<sup>-</sup>, H<sub>3</sub>O<sup>+</sup> and 1 inhibitor molecule was created to simulate the corrosion process as much as possible [24]. The simulation was carried out in a simulation box (24.82 × 24.82 × 35.69 Å<sup>3</sup>) using discover module with a time step of 1 fs and a simulation time of 500 ps performed at 303 K, NVT ensemble (constant number of atoms, constant-volume, constant-temperature) and COMPASS force field [25]. In simulation system, the interactions between inhibitors and Fe (110) surface can be understood by interaction and binding energies calculated using equation (12) and (13) [26]:

$$E_{\text{interaction}} = E_{\text{total}} - (E_{\text{surface+solution}} + E_{\text{inhibitor+solution}}) + E_{\text{solution}} \quad (12)$$

$$E_{\text{Binding}} = -E_{\text{interaction}} \quad (13)$$

where  $E_{\text{total}}$  is the total energy of the entire system  $E_{\text{surface+solution}}$  referred to the total energy of Fe (110) surface and solution without the inhibitor and  $E_{\text{inhibitor+solution}}$  represent the total energy of inhibitor and solution; and  $E_{\text{solution}}$  is the total energy of the solution.

### 3. Results and discussion

#### 3.1 Weight loss measurement

##### 3.1.1 Influence of concentration

Variation of the inhibition efficiency with AIZs concentration is shown in Fig. S3 and several weight loss parameters such as corrosion rate ( $C_R$ ), surface coverage ( $\theta$ ) and corresponding inhibition efficiency (IE %) are listed in Table 2. It is apparent from the results that the inhibition efficiency in presence of AIZs increases with increasing concentration of the studied molecules in 1 M HCl. The studied inhibitors showed maximum inhibition efficiencies of 90%, 93.4% and 96% for AIZ-1, AIZ-2 and AIZ-3, respectively at 0.55 mM concentration. It can be seen from Fig. S3 that after 0.55 mM, no significant change in the inhibition performance was observed indicating that 0.55 mM is an optimum concentration in each case. The high IE of investigated AIZ molecules is attributed to the presence of two N-atoms,  $\pi$ -electrons and two carboxylate anions, which act as an adsorption centers and can effectively cover the metal surface. The higher inhibition efficiency of the AIZ-3, AIZ-2 as compared to AIZ-1 is attributed to the presence of benzyl and methyl substituents in AIZ-3, AIZ-2, respectively.

##### 3.1.2 Effect of temperature

The variation of IE with temperature is shown in Fig. 3. It is clearly seen from the graph that, IE decreases with rise in temperature from 308 to 338K. The decrease in IE may be attributed to desorption of AIZ molecules from the metal surface at elevated temperature [27].

The temperature effect on corrosion rate ( $C_R$ ) for mild steel in the absence and presence of AIZs can be represented by Arrhenius equation [28]:

$$\log(C_R) = \frac{-E_a}{2.303RT} + \log \lambda \quad (14)$$

where  $A$  is the Arrhenius pre-exponent,  $C_R$  is the corrosion rate ( $\text{mgcm}^{-2}\text{h}^{-1}$ ),  $T$  and  $R$  are the absolute temperature and universal gas constant, respectively. The activation energy can be calculated by using the slope ( $-\Delta E_a/2.303R$ ) values. The calculated  $E_a$  value for mild steel in blank acid solution is  $28.48 \text{ kJ mol}^{-1}$ , while in the presence of AIZ-1, AIZ-2, AIZ-3 the  $E_a$  values were  $81.33$ ,  $89.43$  and  $101.64 \text{ kJ mol}^{-1}$ , respectively (Table 3). The increased values of  $E_a$  in the presence of AIZ molecules is attributed to increased energy barrier for the mild steel dissolution in acid solution.

### 3.1.3. Adsorption isotherm

Adsorption isotherm gives the fundamental information about the interaction between inhibitor and metal surface. The AIZ molecules adsorb on metal/solution interface by the displacement of water molecules as shown [29]:



where,  $n$  is the number of water molecules replaced from mild steel surface by each inhibitor molecule. The surface coverage values were used to fit different commonly used adsorption isotherms such as Langmuir, Temkin and Freundlich adsorption isotherms. The Langmuir adsorption isotherm gave the best fit in the present study and is represented in Fig. 4, while Temkin and Freundlich adsorption isotherms are presented in Fig. S4. The values of slope, intercept and regression coefficient are listed in Table S1. The Langmuir adsorption isotherm can be represented as follows:

$$\frac{C}{\theta} = \frac{1}{K_{ads}} + C \quad (16)$$

where,  $C$  is the concentration of inhibitor,  $\theta$  is the fraction of surface coverage and  $K_{ads}$  is the adsorption equilibrium constant. A plot  $C/\theta$  vs.  $C$  (optimum concentration of AIZ molecules) gave a straight line with regressive coefficient ( $R^2$ ) values near to one at  $308 \text{ K}$  (Fig. 4). The

slopes of the straight lines are unity, which indicates that AIZ molecules form a monolayer on the mild steel surface [30]. The values of  $K_{\text{ads}}$  were derived from the intercept ( $1/K_{\text{ads}}$ ) and using the value of  $K_{\text{ads}}$ ,  $\Delta G_{\text{ads}}$  values were calculated by using the following equation [31, 32].

$$\Delta G_{\text{ads}}^{\circ} = -RT \ln(55.5K_{\text{ads}}) \quad (17)$$

where,  $R$  is the universal gas constant,  $T$  is the experimental temperature in Kelvin, 55.5 is the concentration of water in acid solution in mol/L. The adsorption parameters  $\Delta G_{\text{ads}}$ ,  $K_{\text{ads}}$  are listed in Table 3. The negative values of  $\Delta G_{\text{ads}}$  indicated that the studied inhibitors are spontaneously adsorbed onto the mild steel surface [33]. In general, values of  $\Delta G_{\text{ads}}$  around  $-20 \text{ kJ mol}^{-1}$  or more positive are associated with the electrostatic interaction between the opposite charge of AIZ molecules and metal (i.e. physisorption) and  $\Delta G_{\text{ads}}$  values around  $-40 \text{ kJ mol}^{-1}$  or more negative are related to sharing or transferring of electrons between the AIZ molecules and metals surface to form a covalent type bond (i.e. chemisorption) [34, 35]. In the present study, the value of  $\Delta G_{\text{ads}}$  for AIZs ranges from  $-37$  to  $-37.7 \text{ kJ mol}^{-1}$  which are more close to  $-40 \text{ kJ mol}^{-1}$  which signifies that inhibitors are predominantly adsorbed by chemisorption mood [36].

## 3.2 Electrochemical study

### 3.2.1 Potentiodynamic polarization study

The potentiodynamic polarization curves of mild steel in 1 M HCl solution at  $35^{\circ}\text{C}$  without and with different concentrations of AIZ molecules are shown in Fig. 5. The electrochemical parameters such as corrosion potential ( $E_{\text{corr}}$ ), corrosion current density ( $i_{\text{corr}}$ ), anodic and cathodic Tafel slope ( $\beta_{\text{a}}$ ,  $\beta_{\text{c}}$ ) along with the percentage of inhibition efficiency (%IE) are listed in Table 4. Polarization results (Table 4, Fig. 5) show that increase in the AIZs concentration reduces anodic and cathodic currents suggesting that all the three zwitterions are good inhibitors. The maximum decrease in current density from 1150 to  $95 \mu\text{A/cm}^2$  was observed for AIZ-3 indicating that AIZ-3 is the best inhibitor. The order of efficiencies was found  $\text{AIZ-3} > \text{AIZ-2} > \text{AIZ-1}$ . The presence of methyl group in AIZ-2 is resulted in its higher inhibition performance as compared to the AIZ-1. The highest inhibition efficiency of AIZ-3 among the tested compounds is attributed to the presence of benzyl groups. More than 85 mV

shift in the values of  $E_{\text{corr}}$  in the presence of studied compounds, particularly for AIZ-1 indicate that studied molecules behaved as cathodic type. On the basis of polarization study, inhibitor molecules can be classified as anodic, cathodic or mixed type depending upon the displacement in the values of  $E_{\text{corr}}$  with respect to the  $E_{\text{corr}}$  value of uninhibited metallic specimen. In the present case, maximum displacements in the  $E_{\text{corr}}$  values were 98, 77 and 81 mV, indicating that AIZ-1 acts as cathodic type inhibitor, while remaining two behave as mixed type corrosion inhibitors [37]. This finding was further supported by relatively more shifts in the values of  $\beta_c$  as compared to the values of  $\beta_a$ . Inspection of the Fig. 5 reveals that potentiodynamic polarization curves are parallel and similar in the absence and presence of different concentrations of the studied inhibitors indicating that these molecules inhibit metallic corrosion by blocking the active sites present over the metallic surface without changing the mechanism of mild steel corrosion [38].

### 3.2.2 Electrochemical impedance spectroscopy study

Fig. 6 and 7 show the Nyquist and Bode plots for mild steel with and without different concentrations of AIZs. Nyquist plots consist of a depressed capacitive loop along with the real axis and their size increases with increasing the concentration of inhibitor molecules (Fig. 6), indicating that the corrosion of mild steel in 1M hydrochloric acid solution is controlled by polarization resistance ( $R_p$ ) [39]. For a metal corroding in acidic solution,  $R_p$  is associated with several types of resistances such as film resistance ( $R_f$ ), pore resistance ( $R_r$ ), charge transfer resistance ( $R_{ct}$ ) and diffuse layer resistance ( $R_d$ ) etc. that is  $R_p = R_f + R_r + R_{ct} + R_d$  [39]. This finding suggests that mild steel corrosion inhibition occurs by adsorption of AIZ molecules at metal/electrolyte interfaces. The equivalent circuit model used to interpret the impedance results is given in Fig. 5. It consists of solution resistance ( $R_s$ ), polarization resistance ( $R_p$ ) and constant phase element (CPE) [40]. CPE is used in place of capacitor in order to accurately fit the circuit. CPE can be represented by the following equation:

$$Z_{\text{CPE}} = \left( \frac{1}{Y_0} \right) [(j\omega)_n]^{-1} \quad (18)$$

where,  $Y_0$  and  $n$  are the magnitude and exponent (phase shift) of the CPE, respectively,  $j^2 = -1$  is an imaginary number and  $\omega$  is the angular frequency. Properties of CPE depends on the value

of  $n$ . From the Table 5, it can be seen that the values of  $n$  vary from 0.827 to 0.886, which suggest that the surface inhomogeneity decreases due to adsorption of AIZ molecules on the mild steel surface [41]. The values of EIS parameters such as  $R_p$ , CPE,  $Y_0$  and  $n$  obtained by fitting the EIS spectra are listed in Table 5. The values of  $C_{dl}$  can be calculated from the CPE parameters  $Y$  and  $n$  using the following equation:

$$C_{dl} = \frac{Y\omega^{n-1}}{\sin(n(\pi/2))} \quad (19)$$

As shown in Table 5, the value of  $R_p$  increases and  $C_{dl}$  decreases with increasing the inhibitor concentration, which is attributed to increase in the thickness of the electric double layer on the metal/solution interface and/or decrease in the value of dielectric constant due to the displacement of pre-adsorbed water molecules by the inhibitors. From Table 5, the inhibition performance order of AIZ molecules is AIZ-3 > AIZ-2 > AIZ-1. The same trend was obtained from the weight loss and potentiodynamic polarization methods.

The increase in surface smoothness in the presence of AIZ molecules was further supported by Bode plot. It can be seen from the Fig. 7 and Table S2 that phase angle ( $\alpha^0$ ) increases with increase in inhibitors' concentration and maximum increase in phase angle was  $-66.5^0$  at optimum concentration. However, for the ideal capacitor, the phase angle value is  $-90^0$  and constant slope is -1. In the present study, the values of slope range from -0.4805 to -0.7710 and the phase angle ranges from  $-41.30$  to  $-66.50^0$ , respectively. This finding suggests that in the present analysis, mild steel interface did not behave as an ideal capacitor. The deviation from the ideal capacitive behavior in is attributed to surface roughness [42].

### 3.3 Surface study

#### 3.3.1 SEM/EDX analysis

Scanning electron microscopic (SEM) images of uninhibited and inhibited mild steel surfaces in 1 M HCl solution are shown in Fig. 8. Fig. 8a represents the SEM image of the uninhibited metallic specimen which is drastically damaged and corroded due to free acid attack in the absence of inhibitors. However, in the presence of inhibitors at their optimum concentration, the surface morphologies of the metallic specimens (Fig. 8b-d) were remarkably improved, due to

the formation of the protective film by AIZ molecules on the metallic surface which separates the metals from corrosive environments and protects from corrosion. The adsorption of inhibitors molecule on mild steel surface was further supported by EDX spectra of mild steel (Fig. S5). The EDX spectrum of uninhibited metallic specimen (Fig. S5a) shows the presence of oxygen which is attributed to the slow atmospheric oxidation of metallic surface and formation of oxides film ( $\text{Fe}_2\text{O}_3$ ,  $\text{Fe}_3\text{O}_3$ ) during SEM/EDX analyses. However, the EDX spectra of inhibited metallic specimens shown in Fig. S5b-d, give additional signal for nitrogen, which implies that the investigated AIZ molecules are adsorbed on the metallic surface thereby forming a protective surface film preventing further corrosion.

### 3.3.2 AFM analysis

The three-dimension AFM micrographs of these specimens in the absence and presence of inhibitors are depicted in Fig. 9. In the absence of AIZ molecules (Fig. 9a), the metallic surface was highly corroded and damaged owing to the free acidic corrosion. The calculated average surface roughness for uninhibited specimen was 392 nm. However, in the presence of AIZ molecules at their optimum concentration (0.55 mM), average surface roughness was 69 nm (AIZ-1), 45 nm (AIZ-2) and 29 nm (AIZ-3) (Fig. 9b-d) due to the adsorption of inhibitor molecules.

## 3.4. Theoretical studies

### 3.4.1 Quantum chemical calculation

Quantum chemical study using DFT method is an important theoretical tool to study the reactivity of the inhibitor molecules [43]. AIZ molecules exist in cationic and anionic forms depending upon the pH of the medium [44, 45]. In highly acidic solution such as 1M HCl, these molecules exist predominantly in protonated forms. The protonation of carboxylic O-atom of AIZs molecule was done on the basis of Mulliken charge (Mulliken charge on O-atom (-0.459) > N-atom (-0.369)). In view of this, DFT based quantum chemical calculations were carried out for protonated forms of AIZ molecules in aqueous phase. The geometrically optimized structures are

depicted in Fig. 10 and HOMOs, LUMOs with contour and molecular electrostatic potential (MEP) of protonated form of AIZ molecules are shown in Figs.11. The quantum chemical parameters such as  $E_{\text{HOMO}}$ ,  $E_{\text{LUMO}}$ ,  $\Delta E = E_{\text{HOMO}} - E_{\text{LUMO}}$ , hardness ( $\eta$ ), softness ( $\sigma$ ), electronegativity ( $\chi$ ), electrophilicity ( $\omega$ ), nucleophilicity ( $\epsilon$ ) and the fraction of electrons transferred ( $\Delta N_{110}$ ) for protonated form of inhibitors are presented in Table 6.

The inhibition effect of inhibitor molecule is usually attributed to the adsorption of AIZ molecules on the metal surface. The analysis of frontier molecular orbital (HOMO and LUMO) is useful to predict the adsorption center of AIZ molecules responsible for the interaction with metal surface [46]. HOMO and LUMO are associated with the electron donor and acceptor ability of AIZ molecules, respectively. Molecules with higher value of  $E_{\text{HOMO}}$  (less negative) and lower value of  $E_{\text{LUMO}}$  (more negative) show more donor and acceptor tendency of electrons with appropriate metal d-orbital, respectively [47]. From Fig. 11, it can be observed that HOMO are distributed over the imidazole ring in all the AIZ molecules. Therefore, the imidazole ring is responsible for donating the electron to the available vacant 3d orbital of Fe (110). LUMOs are mainly distributed over the carboxylic group of the inhibitor molecules.

The reactive sites of inhibitors were further confirmed by the study of molecular electrostatic potential (MEP). MEP is made the electron density visible and is a useful tool to understanding sites of electrophilic and nucleophilic attack [48]. In MEP, the red (negative) regions are subjected to nucleophilic attack, while blue (positive) regions are related to the electrophilic reactivity. Fig. 11, red and blue region of MEPs are corresponding to the HOMO and LUMO orbital distribution of inhibitor molecules, respectively.

Generally, higher the value of  $E_{\text{HOMO}}$  suggests the better donor performance of inhibitor molecules. Table 6, shows that the values of  $E_{\text{HOMO}}$ ,  $E_{\text{LUMO}}$  and  $\Delta E$  for studied inhibitors in their protonated form obeyed the order AIZ-3 > AIZ-2 > AIZ-1, which supports the order of inhibition efficiencies obtained experimentally. The electronegativity ( $\chi$ ) is another important parameter in order to compare the inhibition efficiencies of structurally similar molecules. According to Pearson, when two systems are brought in contact together, electron transfer will occur from lower  $\chi$  to higher  $\chi$  until the chemical potential become equal [49]. Results showed that the electronegativity of all the three protonated AIZ molecules is between 1.74-1.86 eV, those that are lower than the work function of Fe (110) (4.8 eV). Hence, it is predicted that in the case of protonated AIZ molecules, the AIZ molecules are mainly adsorbed on the metal surface of Fe

(110) by the transfer of electrons from the metal orbitals to the suitable vacant inhibitor orbitals. The values of electronegativity for the studied molecules obeys the trend: AIZ-3 > AIZ-2 > AIZ-1, which is in good agreement with the order of experimentally obtained inhibition efficiency. Electrophilicity ( $\omega$ ) is another important index to measure the electron-accepting ability of inhibitor molecules and is physically related to nucleophilicity ( $\epsilon$ ) according to the relationship given in Eq. (10). Therefore, a molecule with lower value of  $\epsilon$  and higher value of  $\omega$  is likely to behave as good corrosion inhibitor [50]. From the Table 6, it was observed that both the electrophilicity and nucleophilicity are supported by the experimental results.

### 3.4.2 Molecular dynamics (MD) simulation

MD simulations have been done to further study the interactions between tested inhibitors and Fe (110) surface in the presence of all the concerned species, such as water molecules, Cl<sup>-</sup>, H<sub>3</sub>O<sup>+</sup> and one molecule of the investigated compounds. Based on the above discussion, in DFT calculations, MD simulations were performed only using the protonated form of inhibitors. The system reaches equilibrium only when energy and temperature fluctuation have reached their balanced state [51]. When the adsorption process has reached equilibration, the interaction and binding energies between tested inhibitors and Fe (110) surface can be calculated using the equation (12) and (13). Table 7 listed the values of calculated energies. Fig. 12 presents side and top views of the adsorption configuration of tested inhibitors derived from MD simulations. By inspection of this figure, it could be observed that the investigated compounds adsorb nearly to Fe (110) surface, where chemical bonds can possibly occur through heteroatoms and  $\pi$ -electrons in phenyl rings. Looking at Fig. 12, it is apparent that in the case of AIZ-1 and AIZ-2, the carboxyl groups are directed towards the solvent layer whereas the imidazolium ring moving almost parallel to the surface suggesting that the significant interactions can occur between nitrogen atoms and iron surface. In the case of AIZ-3, the phenyl ring covered more surface area of the metal, likely due to the presence of  $\pi$ -electrons, on the other side, although the interactions between the phenyl ring and metal surface are seen to be insignificant, the oxygen-iron interactions may thus be the most important on this side. It can thus be suggested that the active sites from phenyl ring and oxygen atoms are mainly responsible for the increase in the inhibition efficiency. Otherwise, it can be seen from the data in Table 7 that the binding energies of the

adsorption of inhibitors on Fe (110) surface are very high and positive suggesting the high stability of the adsorbed inhibitors [52, 53]. The higher negative values of interaction energy can be attributed to the strong adsorption of AIZ molecules on the Fe surface [54].

The radial distribution function (RDF) (or pair correlation function)  $g(r)$  is an effective and useful method to estimate the bond length. The first peak occurs at  $1 \text{ \AA} \sim 3.5 \text{ \AA}$ , indicating the chemisorption whereas the physisorption is associated with the peaks longer than  $3.5 \text{ \AA}$  [52, 55]. The radial distribution function of C, O and N atoms of AIZ-3 graphically presented in Fig. 13 shows that all the bond length of Fe-C ( $3.1 \text{ \AA}$ ), Fe-N ( $3.1 \text{ \AA}$ ) and Fe-O ( $2.9 \text{ \AA}$ ) are less than  $3.5 \text{ \AA}$ , so chemical interactions can occur between these atoms and the metallic surface.

As mentioned in the DFT calculations, once again it can be inferred that the protonated form of the tested inhibitors plays a crucial role in the corrosion inhibition process.

#### 4. Conclusion

In the present study, inhibition behavior of three amino acid derived imidazolium zwitterions (AIZs) have been investigated by experimental and theoretical methods. Following conclusions have been drawn:

- (1) Both experimental and theoretical studies suggest that the studied imidazolium based zwitterions act as good corrosion inhibitors for mild steel corrosion in 1 M HCl and their inhibition efficiency increases with increase in concentration. The maximum values of % IE for AIZ-1, AIZ-2 and AIZ-3 were 90%, 93.4% and 96%, respectively at concentration as low as 0.55 mM (200 ppm).
- (2) The studied zwitterions inhibit corrosion by adsorbing on the metallic surface at which the adsorption obeyed the Langmuir isotherm.
- (3) The results of potentiodynamic polarization study reveal that AIZ-1 acts as predominantly cathodic type inhibitor while AIZ-2 and AIZ-3 behave as mixed type inhibitors.
- (4) The EIS study reveals that the studied zwitterions inhibit mild steel corrosion by getting adsorbed at the metal/electrolyte interfaces thereby forming the surface protective film which isolates the metals from the corrosive environment. The increased values of  $R_p$  and decreased values of  $C_{dl}$  justify the observation.

- (5) The adsorption and film forming ability of the studied inhibitor molecules on the metallic surface were supported by SEM, EDX and AFM analyses.
- (6) Quantum chemical calculation results show that protonated inhibitors are better inhibitors than the neutral inhibitors. The results of DFT parameters corroborated with experimental results and a good agreement has been observed between them.
- (7) Molecular dynamics simulation results reveal that inhibitor molecules adsorbed through flat orientation and their order of effectiveness followed the experimental order of inhibition efficiency.

### Acknowledgements

Haque and Verma thankfully acknowledge the Ministry of Human Resource Development (MHRD) and central instrumental facility center (CIFC) IIT (BHU) Varanasi for providing financial and instrumental support, respectively.

### References:

- [1] G.H. Koch, N.G. Thompson, O. Moghissi, J.H. Payer, J. Varney, "IMPACT (International Measures of Prevention, Application, and Economics of Corrosion Technologies Study," Report No. OAPUS310GKCOCH (AP110272) (Houston, TX: NACE International, 2016).
- [2] E. Kowsaria, M. Payamia, R. Aminib, B. Ramezanzadehb, M. Javanbakht, Task-specific ionic liquid as a new green inhibitor of mild steel corrosion, *Appl. Surf. Sci.*, 289 (2014) 478–486.
- [3] C. Verma, P. Singh, I. Bahadur, E.E. Ebenso, M.A. Quraishi, Electrochemical, thermodynamic, surface and theoretical investigation of 2-aminobenzene-1,3-dicarbonitriles as green corrosion inhibitor for aluminum in 0.5 M NaOH, *J. Mol. Liq.*, 209 (2015) 767–778.
- [4] Y. Tang, X. Yang, W. Yang, Y. Chen, R. Wan, Experimental and molecular dynamics studies on corrosion inhibition of mild steel by 2-amino-5-phenyl-1,3,4-thiadiazole, *Corros. Sci.*, 52 (2010) 242–249.
- [5] C. Verma, L.O. Olasunkanmi, E.E. Ebenso, M.A. Quraishi, I.B. Obot, Adsorption Behavior of Glucosamine-Based, Pyrimidine-Fused Heterocycles as Green Corrosion

- Inhibitors for Mild Steel: Experimental and Theoretical Studies, *J. Phys. Chem. C*, 120 (2016) 11598–11611.
- [6] M. Bobina, A. Kellenberger, J.-P.C.Millet, N. Muntean, Vaszilcsin, corrosion resistance of carbon steel in weak acid solutions in the presence of l-histidine as corrosion inhibitor, *Corros. Sci.*, 69 (2013) 389–395.
- [7] I. Milosev, J. Pavlinac, M. Hodoscek, A. Lesar, Amino acids as corrosion inhibitors for copper in acidic medium: Experimental and theoretical study, *J. Serb. Chem. Soc.*, 78 (2013) 2069–2086.
- [8] H. Zhao, X. Zhang, L. Ji, H. Hud, Q. Li, Quantitative structure–activity relationship model for amino acids as corrosion inhibitors based on the support vector machine and molecular design, *Corros. Sci.*, 83 (2014) 261–271.
- [9] Sustainable Catalysis: Challenges and Practices for the Pharmaceutical and Fine Chemical Industries, ed. P. J. Dunn, K. K. Hii, M. J. Krische and M. T. Williams, Wiley, Weinheim, 2013.
- [10] R.A. Sheldon, Green and sustainable manufacture of chemicals from biomass: state of the art, *Green Chem.*, 16 (2014) 950–963.
- [11] H. Ashassi-Sorkhabia, M.R. Majidib, K. Seyyedi, Investigation of inhibition effect of some amino acids against steel corrosion in HCl solution, *Appl. Surf. Sci.*, 225 (2004) 176–185.
- [12] M. A. Amin, K.F. Khaled, Q. Mohsen, H.A. Arida, A study of the inhibition of iron corrosion in HCl solutions by some amino acids, *Corros. Sci.*, 52 (2010) 1684–1695.
- [13] M. Mobin, S. Zehra, M. Parveen, L-cysteine as corrosion inhibitor for mild steel in 1MHCl and synergistic effect of anionic, cationic and non-ionic surfactants, *J. Mol.Liq.*, 216 (2016) 598–607.
- [14] D. Zhang, X. He, Q. Cai, L. Gao, G.S. Kim, pH and iodide ion effect on corrosion inhibition of histidine self-assembled monolayer on copper, *Thin Solid Films*, 518 (2010) 2745–2749.
- [15] J. Haque, V. Srivastava, C. Verma, M.A. Quraishi, Experimental and quantum chemical analysis of 2-amino-3-((4-((S)-2-amino-2-carboxyethyl)-1H-imidazol-2-yl)thio)propionic acid as new and green corrosion inhibitor for mild steel in 1 M hydrochloric acid solution, *J. Mol. Liq.*, 225 (2017) 848–855.

- [16] S. Kirchhecker, M. Antonietti, D. Esposito, Hydrothermal decarboxylation of amino acid derived imidazolium zwitterions: a sustainable approach towards ionic liquids, *Green Chem.*, 16 (2014) 3705.
- [17] A.S.D. G1-90, Standard Practice for Preparing, Cleaning and Evaluating Corrosion Test Specimens, ASTM, in, Philadelphia, PA, 1999 (Reapproved 1999).
- [18] J. Haque, K.R. Ansari, V. Srivastava, M.A. Quraishi, I.B. Obot, Pyrimidine derivatives as novel acidizing corrosion inhibitors for N80 steel useful for petroleum industry: A combined experimental and theoretical approach, *J. Ind. Eng. Chem.*, <http://dx.doi.org/10.1016/j.jiec.2017.01.025>.
- [19] M. J.Frisch et al. "Gaussian 09, revision D. 01." (2009).
- [20] C. Lee, W. Yang, R.G. Parr, Development of the Colic-Salvetti correlation-energy formula into a functional of the electron density, *Phys. Rev. B*, 37 (1988) 785–789.
- [21] N. Kovacevic, A. Kokalj, Analysis of molecular electronic structure of imidazole- and benzimidazole-based inhibitors: a simple recipe for qualitative estimation of chemical hardness, *Corros. Sci.*, 53 (2011) 909–921.
- [22] R.G. Parr, L. von Szentpaly, S. Liu, Electrophilicity index, *J. Am. Chem. Soc.*, 121 (1999) 1922.
- [23] Materials Studio, Revision 6.0, Accelrys Inc., San Diego, USA, 2013.
- [24] Z. Salarvand, M. Amirnasr, M. Talebian, K. Raeissi, S. Meghdadi, Enhanced corrosion resistance of mild steel in 1 M HCl solution by trace amount of 2-phenyl-benzothiazole derivatives: Experimental, quantum chemical calculations and molecular dynamics (MD) simulation studies, *Corros. Sci.* 114 (2017) 133–145. doi:10.1016/j.corsci.2016.11.002.
- [25] H. Sun, COMPASS: an ab initio force-field optimized for condensed-phase applications overview with details on alkane and benzene compounds, *J. Phys. Chem. B.*, 102 (1998) 7338–7364.
- [26] Z. Zhang, N.C. Tian, X.D. Huang, W. Shang, L. Wu, Synergistic inhibition of carbon steel corrosion in 0.5 M HCl solution by indigo carmine and some cationic organic compounds: experimental and theoretical studies, *RSC Adv.*, 6 (2016) 22250–22268.
- [27] R. Karthikaiselvi, S. Subhashini, Study of adsorption properties and inhibition of mild steel corrosion in hydrochloric acid media by water soluble composite poly (vinyl alcohol-omethoxy aniline), *JAAUBAS*, (2014) 16, 74–82.

- [28] C. Verma, L.O. Olasunkanmi, I.B. Obot, E.E. Ebenso, M.A. Quraishi, 2,4-Diamino-5-(phenylthio)-5H-chromeno [2,3-b] pyridine-3-carbonitriles as green and effective corrosion inhibitors: gravimetric, electrochemical, surface morphology and theoretical studies, *RSC Adv.*, 6 (2016) 53933.
- [29] P.M. Wadhwan, V.K. Panchal, N.K. Shah, Newly synthesized salicylidene-4,4\_-dimorpholine (SDM) assembled on nickel oxide nanoparticles (NiONPs) and its inhibitive effect on mild steel in 2 N hydrochloric acid, *Appl. Surf. Sci.*, 331 (2015) 373–387.
- [30] V.M. Abbasova, Hany M. Abd El-Lateef, L.I. Aliyeva, E.E. Qasimov, I.T. Ismayilov, Mai M. Khalaf, A study of the corrosion inhibition of mild steel C1018 in CO<sub>2</sub>-saturated brine using some novel surfactants based on corn oil, *Egypt. J. Pet.*, 22 (2013) 451–470.
- [31] I. Ahamada, R. Prasad, M.A. Quraishi, Experimental and quantum chemical characterization of the adsorption of some Schiff base compounds of phthaloylthiocarbonylhydrazide on the mild steel in acid solutions, *Mater. Chem. Phys.*, 124 (2010) 1155–1165.
- [32] A. Ghanbari, M.M. Attar, M. Mahdavian, Corrosion inhibition performance of three imidazole derivatives on mild steel in 1M phosphoric acid, *Mater. Chem. Phys.*, 124 (2010) 1205–1209.
- [33] M. Ebrahimzadeh, M. Gholami, M. Momeni, A. Kosari, M.H. Moayed, A. Davoodi, Theoretical and experimental investigations on corrosion control of 65Cu–35Zn brass in nitric acid by two thiophenol derivatives, *Appl. Surf. Sci.*, 332 (2015) 384–392.
- [34] F. Bentiss, M. Lebrini, M. Lagrenee, Thermodynamic characterization of metal dissolution and inhibitor adsorption processes in mild steel/2,5-bis(n-thienyl)-1,3,4thiadiazoles/hydrochloric acid system, *Corros. Sci.*, 47 (2005) 2915–2931.
- [35] C. Verma, E.E. Ebenso, Y. Vishal, M.A. Quraishi, Dendrimers: A new class of corrosion inhibitors for mild steel in 1MHCl: Experimental and quantum chemical studies, *J. Mol. Liq.*, 224 (2016) 1282–1293.
- [36] E. Kowsari, M. Payami, R. Amini, B. Ramezanzadeh, M. Javanbakht, Task-specific ionic liquid as a new green inhibitor of mild steel corrosion, *Appl. Surf. Sci.*, 289 (2014) 478–486.
- [37] O.L. Riggs Jr., Corrosion Inhibitors, 2nd ed., C.C. Nathan, Houston, TX, 1973.

- [38] Z. Tao, S. Zhang, W. Li, B. Hou, Corrosion inhibition of mild steel in acidic solution by some oxo-triazole derivatives, *Corros. Sci.*, 51 (2009) 2588–2595.
- [39] Resit Yıldız, An electrochemical and theoretical evaluation of 4,6-diamino-2- pyrimidine thiol as a corrosion inhibitor for mild steel in HCl solutions, *Corros. Sci.*, 90 (2015) 544–553.
- [40] A. Popov, E. Sokolova, S. Raicheva, M. Christov, AC and DC study of the temperature effect on mild steel corrosion in acid media in the presence of benzimidazole derivatives, *Corros. Sci.*, 45 (2003) 33–58.
- [41] S.A. Umorena, Y. Li, F.H. Wang, Electrochemical study of corrosion inhibition and adsorption behaviour for pure iron by polyacrylamide in H<sub>2</sub>SO<sub>4</sub>: Synergistic effect of iodide ions, *Corros. Sci.*, 52 (2010) 1777–1786.
- [42] C. Verma, M.A. Quraishi, E.E. Ebenso, I.B. Obot, A. El Assyry, 3-Amino alkylated indoles as corrosion inhibitors for mild steel in 1M HCl: Experimental and theoretical studies, *J. Mol. Liq.*, 219 (2016) 647–660.
- [43] I.B. Obot, D.D. Macdonald, Z.M. Gasem, Density functional theory (DFT) as a powerful tool for designing new organic corrosion inhibitors. Part 1: An overview, *Corros. Sci.*, 99 (2015) 1–30.
- [44] D.C. Silverman, D.J. Kalota, F.S. Stover, Effect of pH on Corrosion Inhibition of Steel by Polyaspartic Acid, *Corros.*, 51 (1995) 818.
- [45] Da-Quan Zhang, Qi-RuiCai, Li-XinGao, K. Y. Lee, Effect of serine, threonine and glutamic acid on the corrosion of copper in aerated hydrochloric acid solution, *Corros. Sci.*, 50 (2008) 3615–3621.
- [46] I. Danaee, O. Ghasemi, G.R. Rashed, M. R. Avei, M.H. Maddahy, Effect of hydroxyl group position on adsorption behavior and corrosion inhibition of hydroxybenzaldehyde Schiff bases: Electrochemical and quantum calculations, *J. Mol. Struct.*, 1035 (2013) 247–259.
- [47] H. Keles, M. Keles, I. Dehri, O. Serindag, The inhibitive effect of 6-amino-m-cresol and its Schiff base on the corrosion of mild steel in 0.5 M HCl medium, *Mater. Chem. Phys.*, 112 (2008) 173–179.

- [48] D. Daoud, T. Douadi, H. Hamani, S. Chafaa, M. Al-Noaimi, Corrosion inhibition of mild steel by two new S-heterocyclic compounds in 1 M HCl: Experimental and computational study, *Corros. Sci.*, 94 (2015) 21–37.
- [49] R.G. Pearson, Absolute electronegativity and hardness: application to inorganic chemistry, *Inorg. Chem.*, 27(1988) 734–740.
- [50] S. Kaya, L. Guo b , C. Kaya, B. Tuzun, I.B. Obot, R. Touir, N. Islam, Quantum chemical and molecular dynamics simulation studies for the prediction of inhibition efficiencies of some piperidine derivatives on the corrosion of iron, *J. Taiwan Inst. Chem. Eng.*, 65 (2016) 522–529.
- [51] H. Lgaz, R. Salghi, S. Jodeh, B. Hammouti, Effect of clozapine on inhibition of mild steel corrosion in 1.0 M HCl medium, *J. Mol. Liq.*, 225 (2017) 271–280.
- [52] S.W. Xie, Z. Liu, G.-C. Han, W. Li, J. Liu, Z. Chen, Molecular dynamics simulation of inhibition mechanism of 3,5-dibromo salicylaldehyde Schiff's base, *Comput. Theor. Chem.*, 1063 (2015) 50–62.
- [53] Z. Zhang, N. Tian, X. Huang, W. Shang, L. Wu, Synergistic inhibition of carbon steel corrosion in 0.5 M HCl solution by indigo carmine and some cationic organic compounds: experimental and theoretical studies, *RSC Adv.*, 6 (2016) 22250–22268.
- [54] S.K. Saha, M. Murmu, N.C. Murmu, P. Banerjee, Evaluating electronic structure of quinazolinone and pyrimidinone molecules for its corrosion inhibition effectiveness on target specific mild steel in the acidic medium: A combined DFT and MD simulation study, *J. Mol. Liq.*, 224 (2016) 629–638.
- [55] Z. Zhang, N. Tian, W. Zhang, X. Huang, L. Ruan, L. Wu, Inhibition of carbon steel corrosion in phase-change-materials solution by methionine and proline, *Corros. Sci.*, 111 (2016) 675–689.

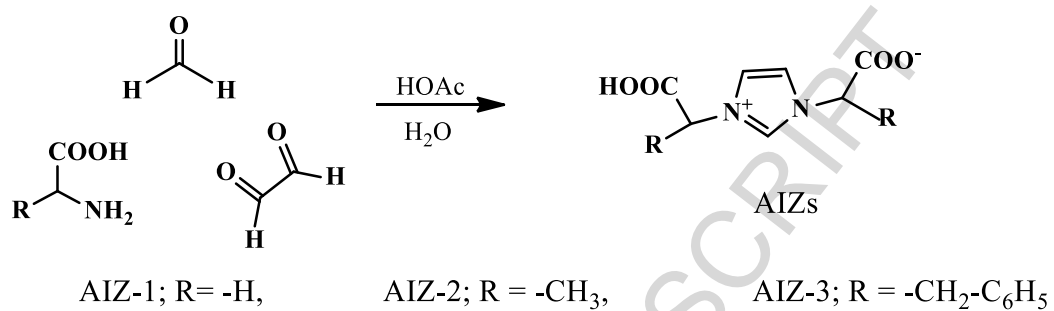


**Fig.1:** Synthetic scheme of studied AIZs.

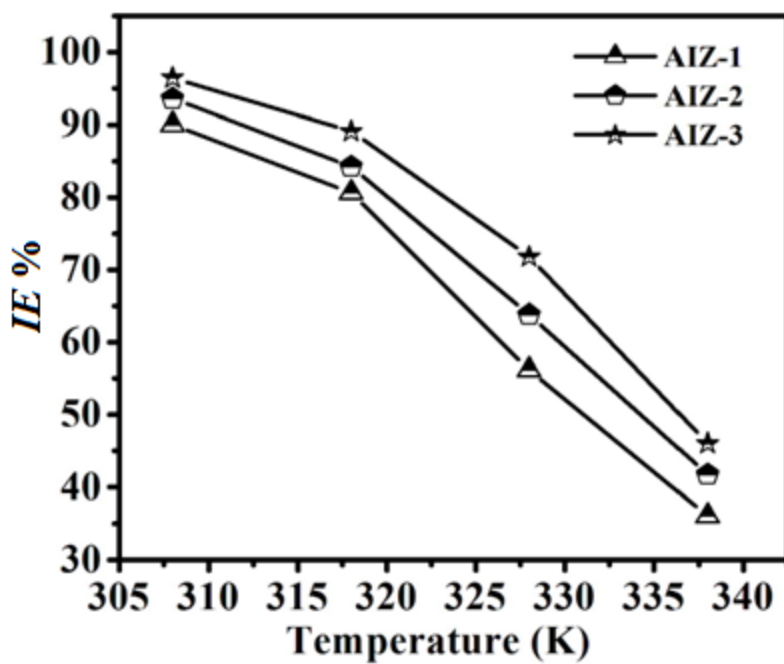


Fig.2: Variation of inhibition efficiency with temperature.

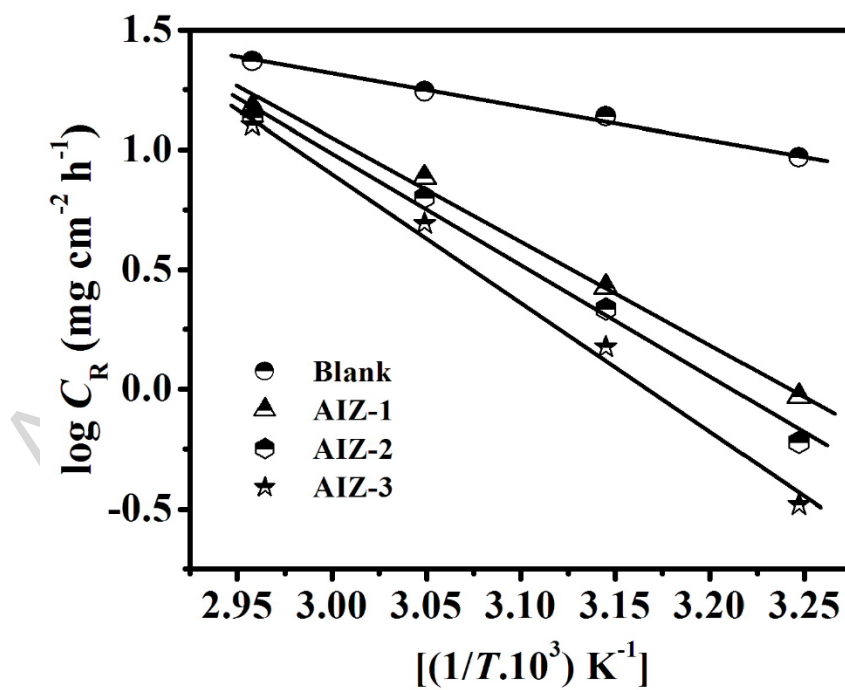


Fig. 3: Arrhenius plots for the corrosion rate of mild steel versus the temperature in 1M HCl.

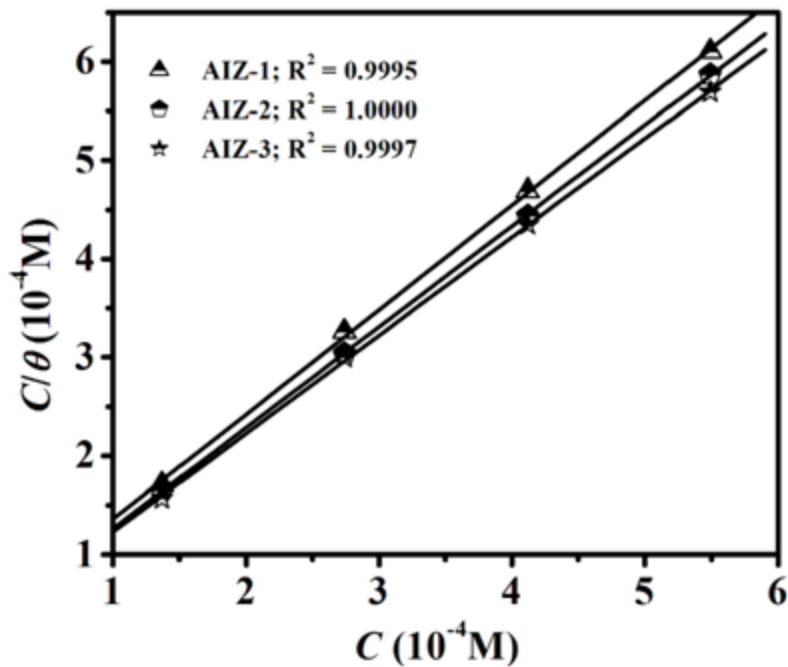
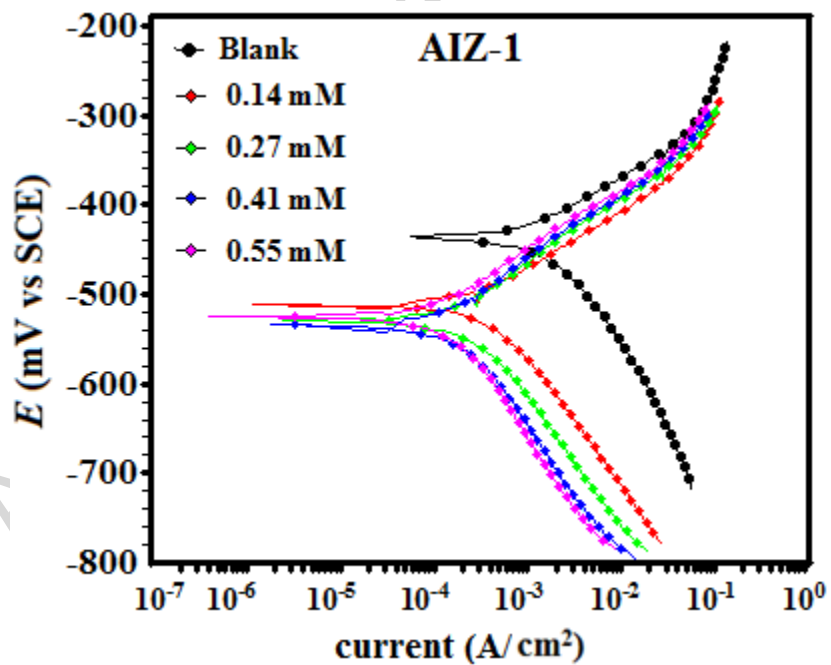
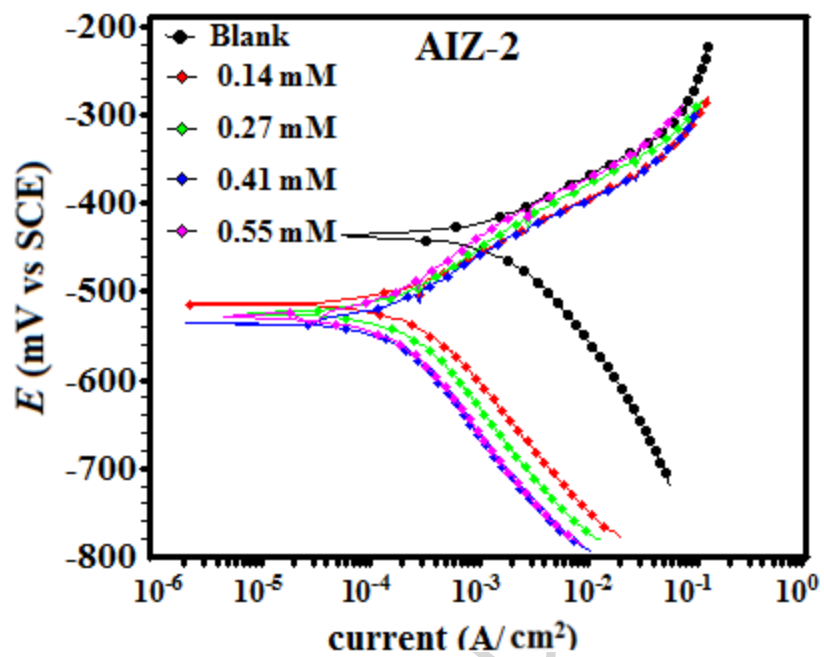
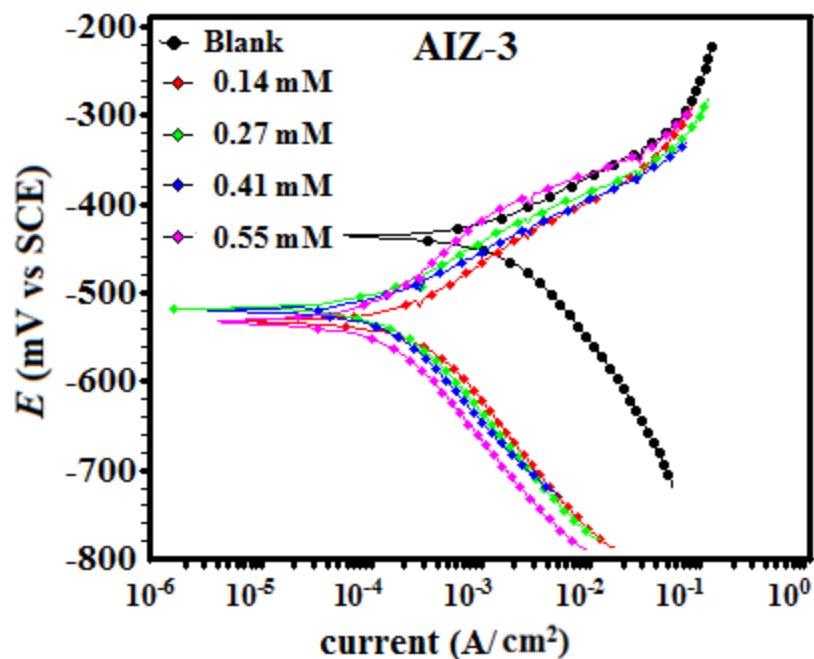


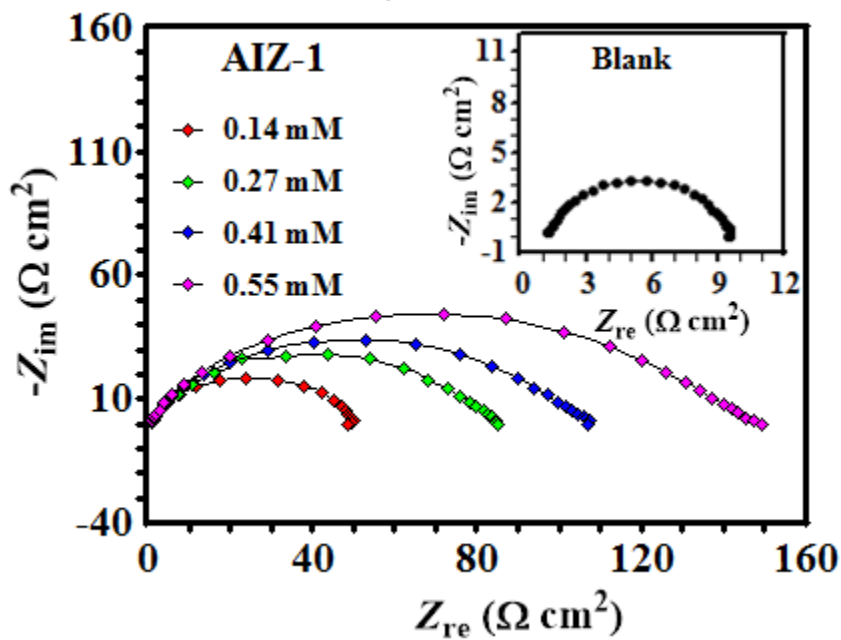
Fig. 4: Langmuir isotherm plot for the adsorption of AIZs on mild steel surface in 1M HCl.







**Fig. 5:** Polarization curves for mild steel in absence and presence of different concentrations of AIZs in 1M hydrochloric acid solution at 308K.



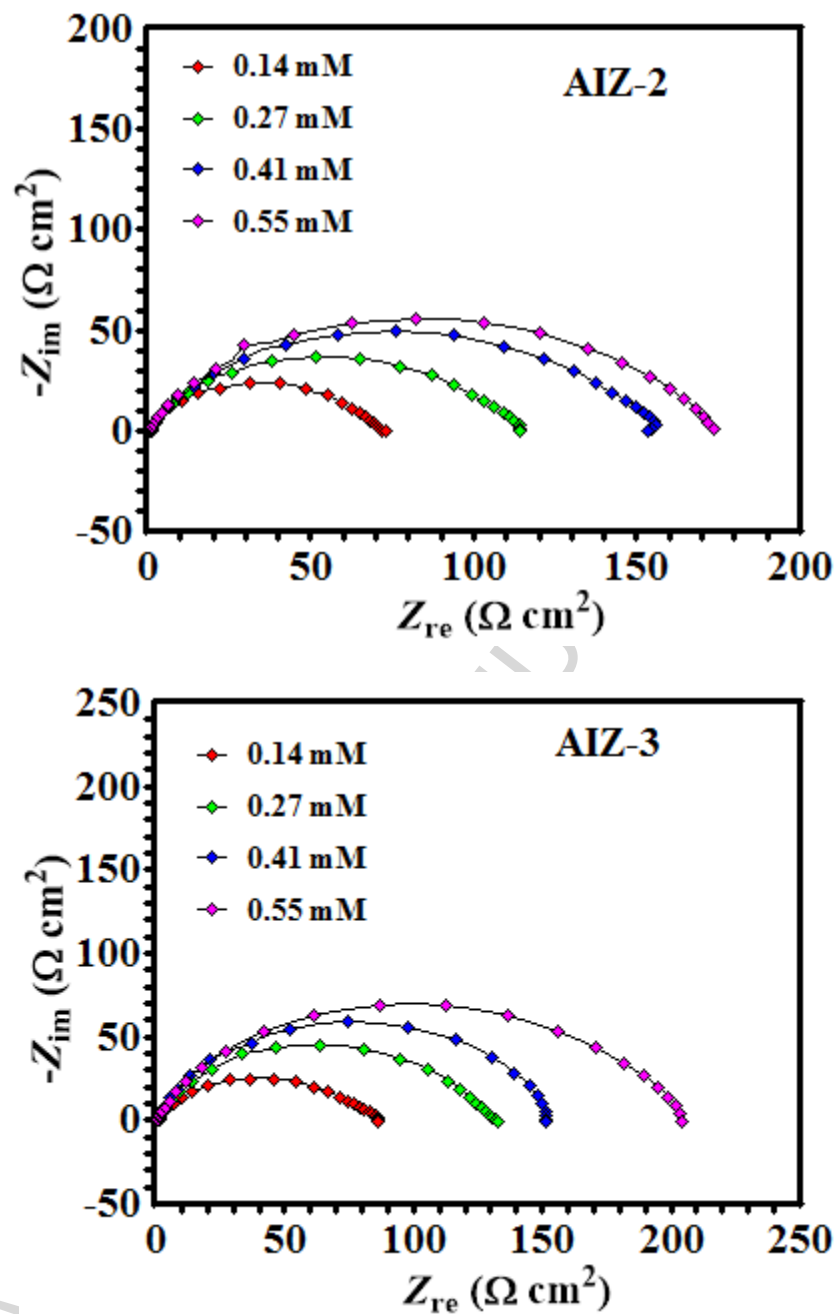


**Fig.6:** Nyquist plot for mild steel in 1 M HCl without and with different concentrations of AIZs at 308K.

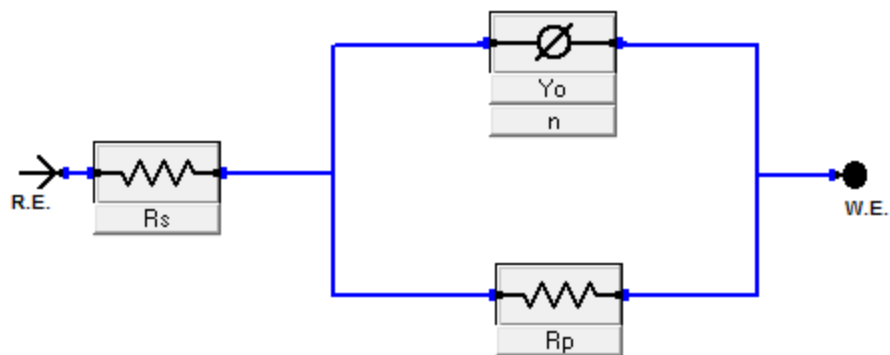
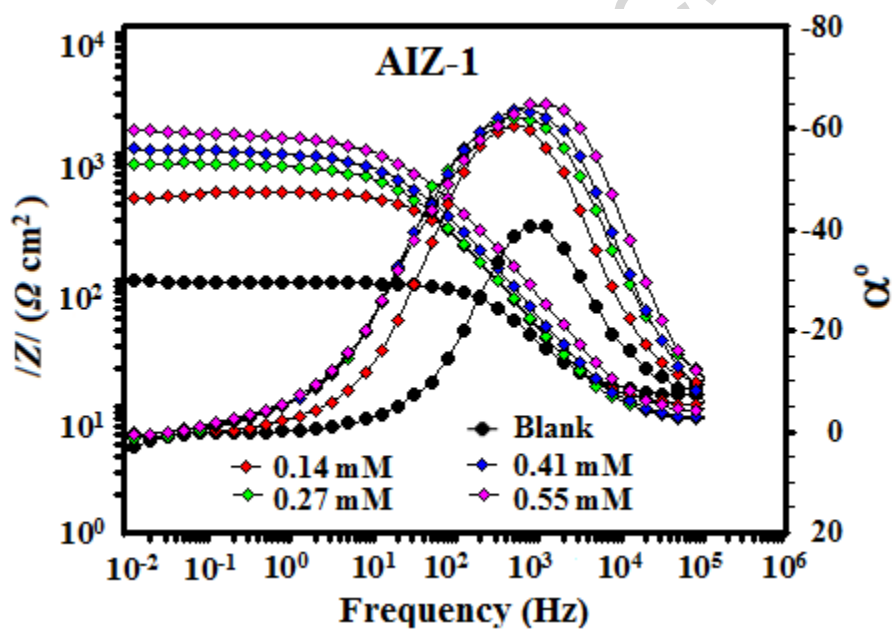
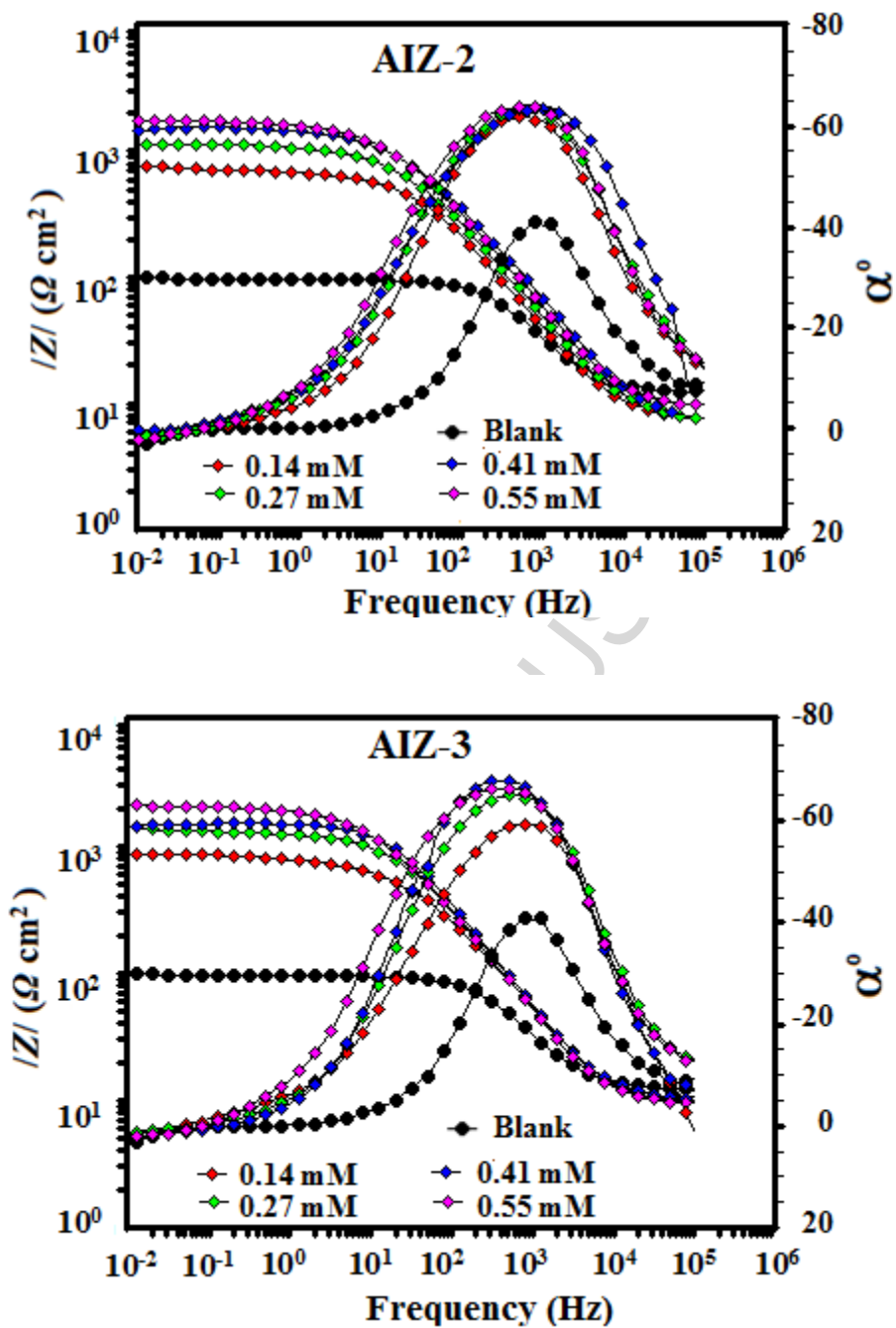
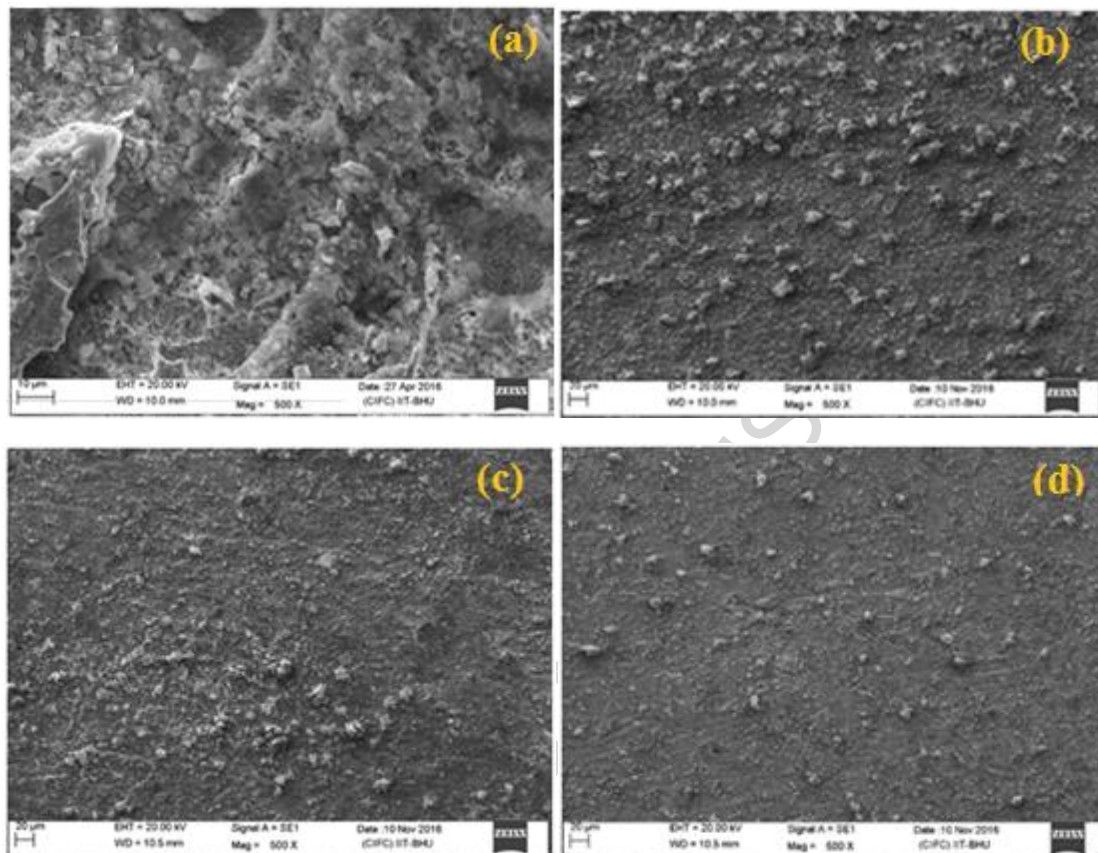


Fig. 7: Equivalent circuit model used for fit and analyzed electrochemical data.





**Fig. 7:** Bode ( $\log f$  vs  $\log |Z|$ ) and phase angle ( $\log f$  vs.  $\alpha^0$ ) plots for mild steel in 1 M HCl in absence and presence of different concentration of AIZs.



**Fig.8:** SEM images of mild steel: (a) in absence of AIZs and in the presence of 0.55 mM of (b) AIZ-1, (c) AIZ-2, and (d) AIZ-3.

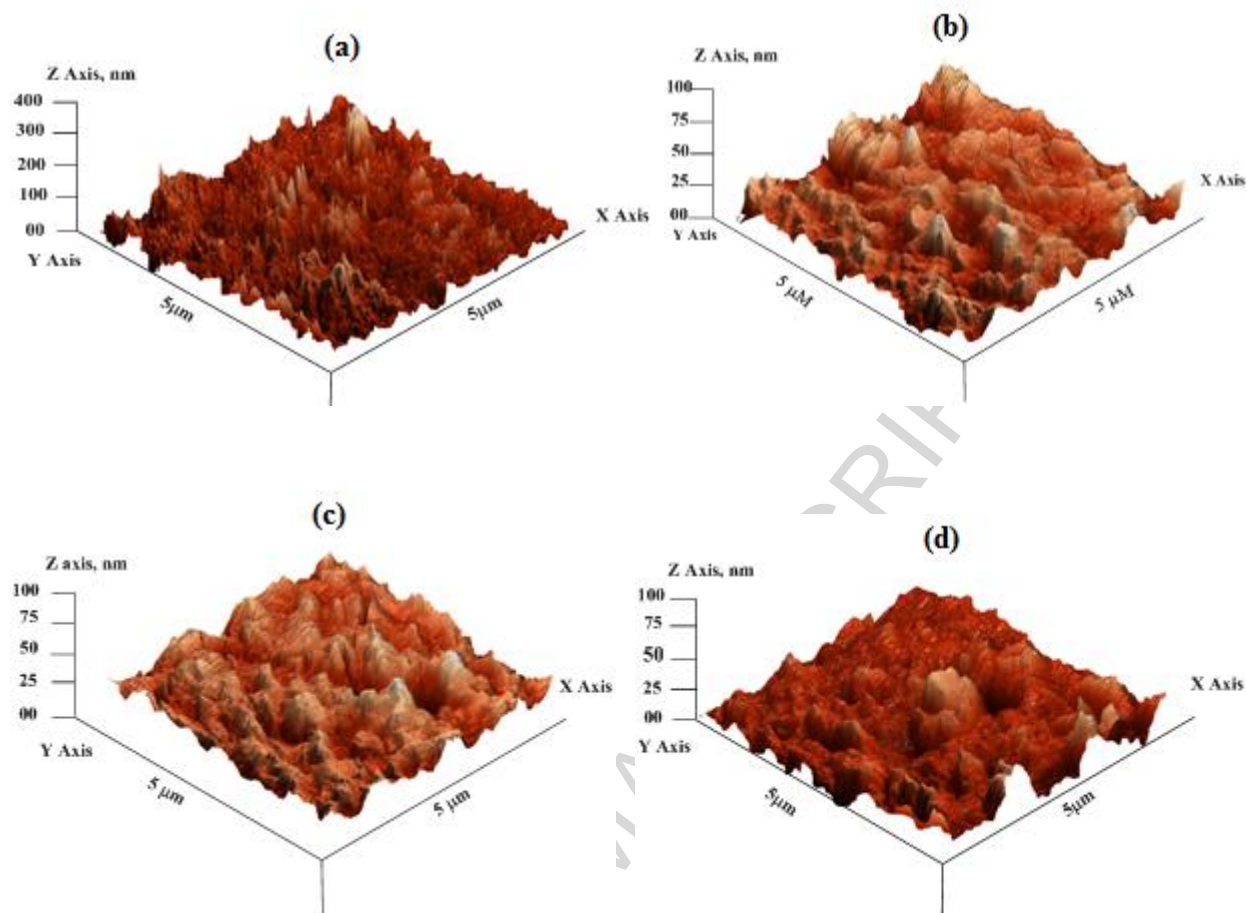


**Fig. 9:** AFM images of mild steel: (a) in absence of AIZs and in the presence of 0.55 mM of (b) AIZ-1, (c) AIZ-2, and (d) AIZ-3.

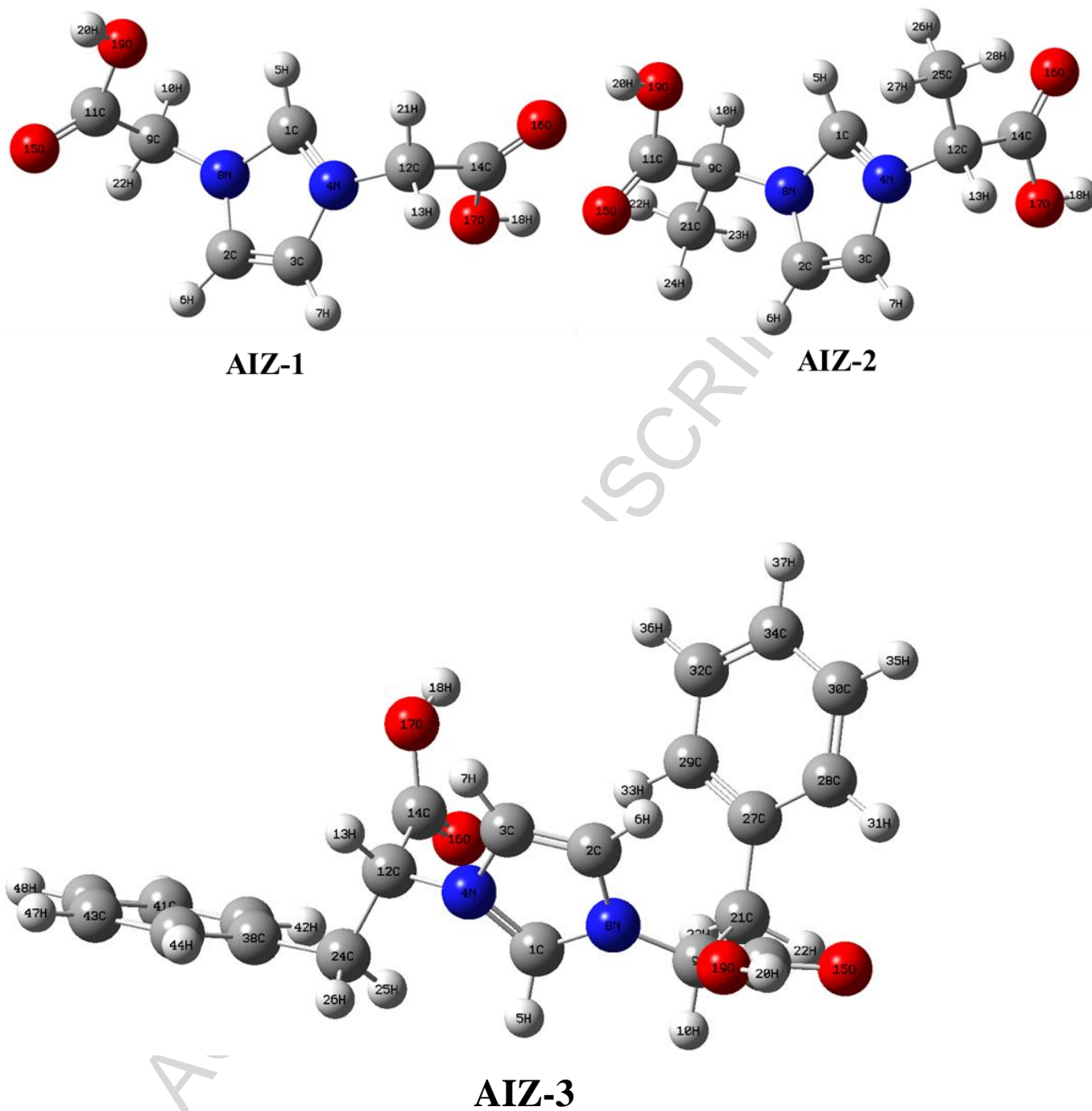


**Fig.10** The optimized structures of protonated AIZ inhibitors.

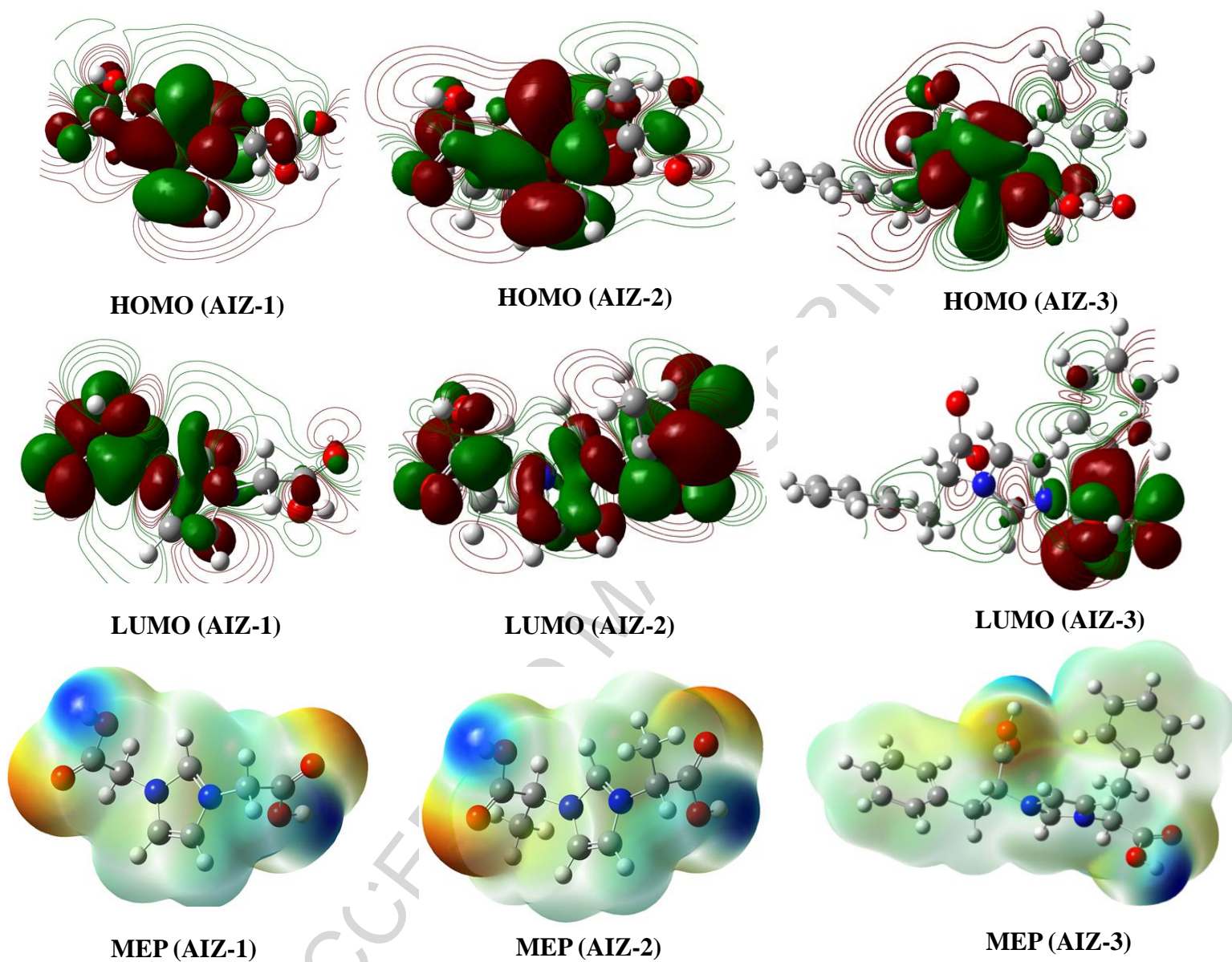
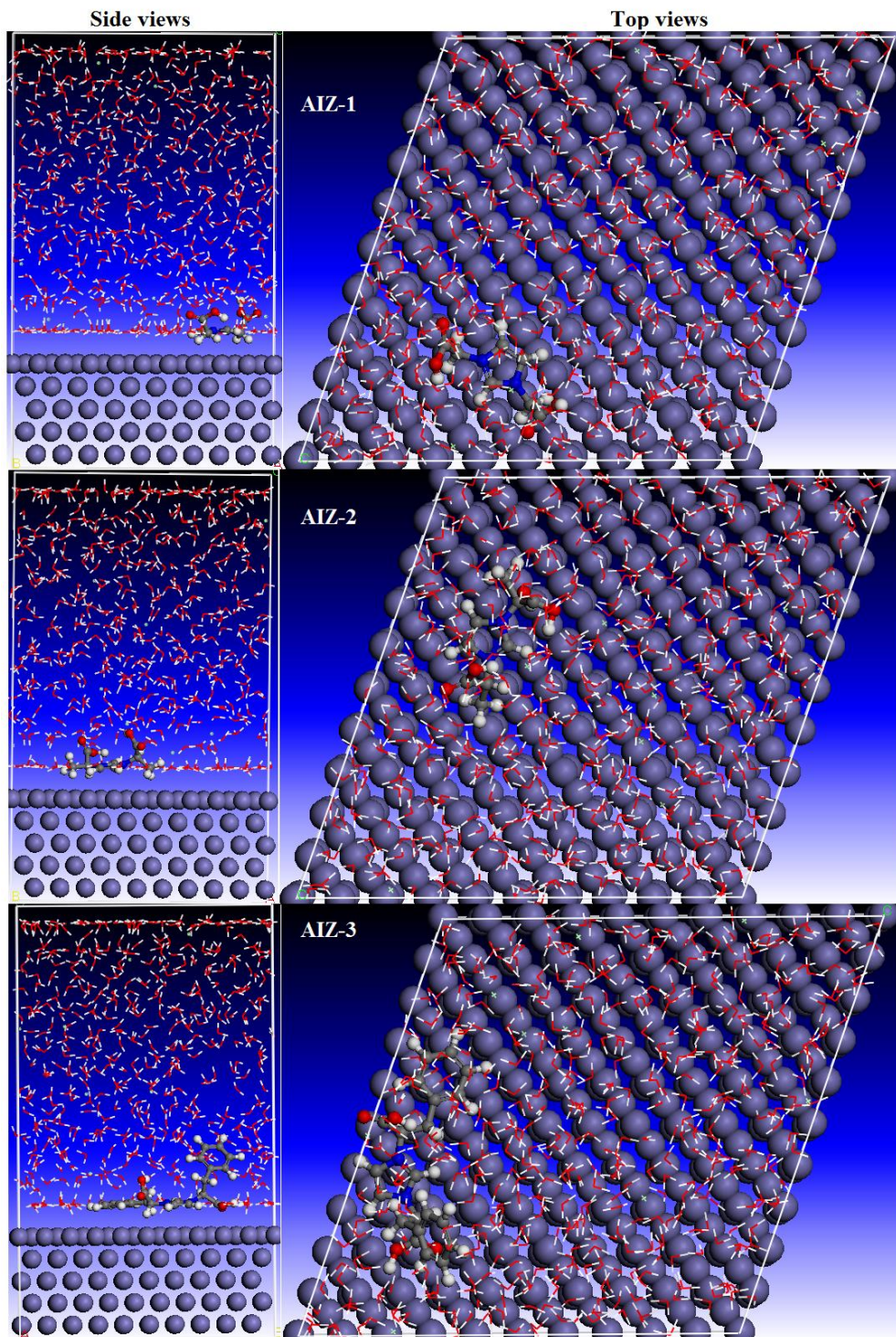
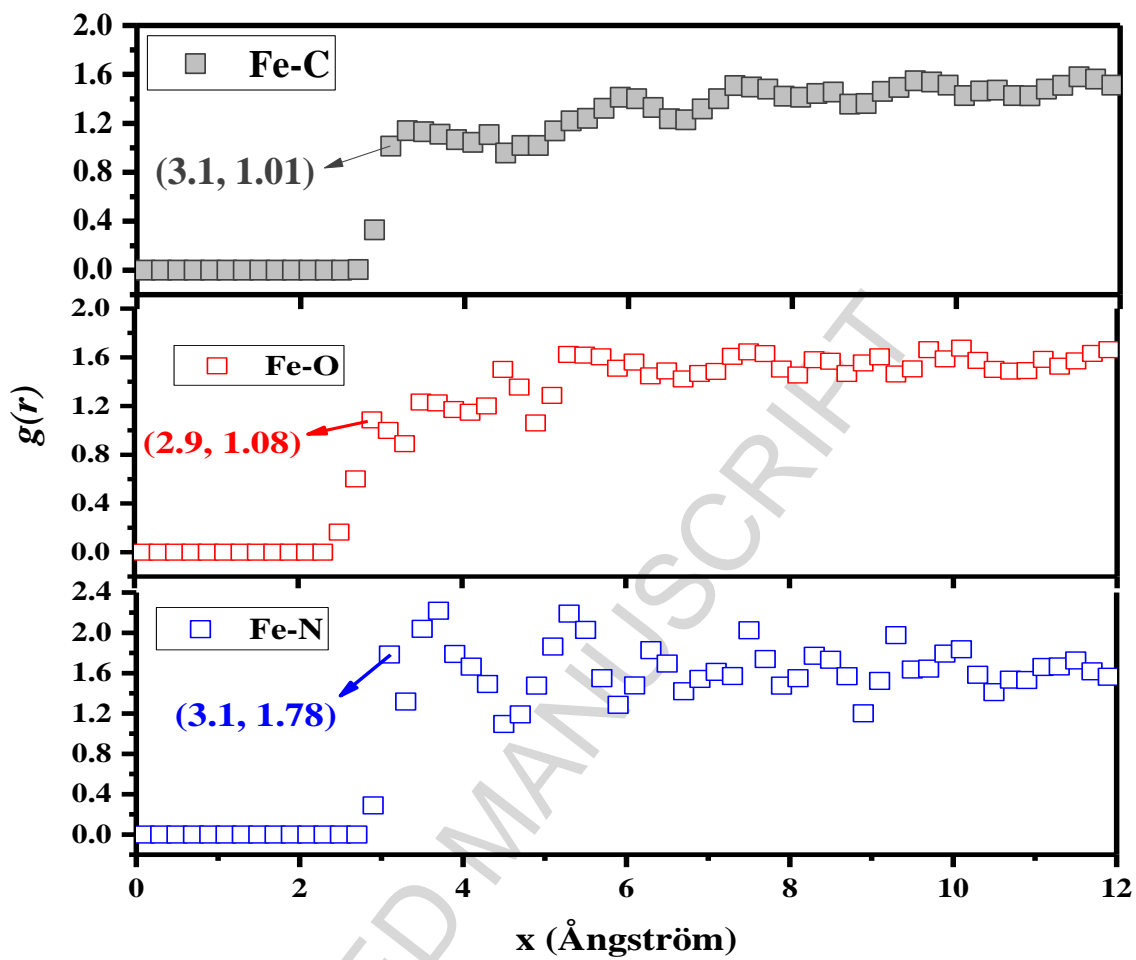


Fig. 11: The HOMOs, LUMOs and molecular electrostatic potential (MEP) structures of protonated AIZ inhibitors.

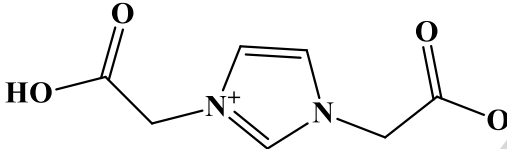
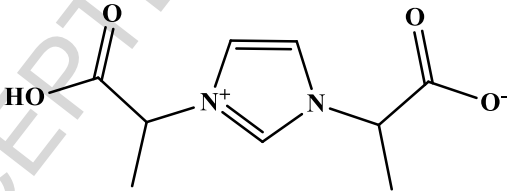


**Fig. 12:** Top and side views of the final adsorption of the tested inhibitors on the Fe (110) surface in solution.



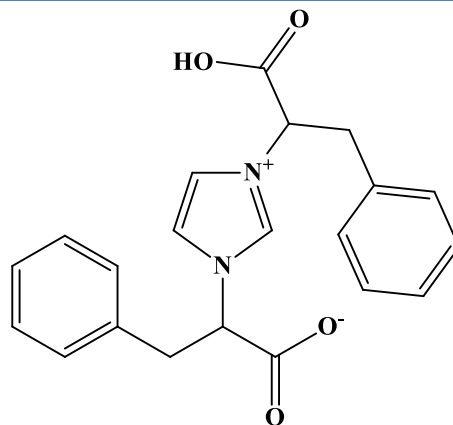
**Fig. 13:** Radial distribution functions of AIZ-3 adsorbed on a Fe (110) surface.

**Table 1:** IUPAC name, molecular structure, molecular formula and melting point of the synthesized inhibitor molecules (AIZs).

S.No.	IUPAC name and Abbreviation of Inhibitor	Chemical structure	Molecular formula, M.P. and Characterization data
1	2-(3-(carboxymethyl)-1H-imidazol-3-ium-1-yl)acetate (AIZ-1)		C <sub>7</sub> H <sub>8</sub> N <sub>2</sub> O <sub>4</sub> (mol. wt. 184.15) M.P. 290 °C, IR $\nu_{\max}/\text{cm}^{-1}$ = 3292 (C-H), 3068 (C-O), 1643 (C=O), 1212 (OH), 638, <sup>1</sup> H-NMR (500 MHz, D <sub>2</sub> O) $\delta_{\text{H}}$ 8.89 (s, 1H, ArH), 7.45 (s, 2H ArH), 4.95 (s, 4H, CH <sub>2</sub> ), <sup>13</sup> C-NMR (126 MHz, D <sub>2</sub> O) $\delta_{\text{C}}$ 170.9, 137.7, 123.3, 51.0.
2.	2-(3-(1-carboxyethyl)-1H-imidazol-3-ium-1-yl)propanoate (AIZ-2)		C <sub>9</sub> H <sub>12</sub> N <sub>2</sub> O <sub>4</sub> (mol. wt. 212.21) M.P. 218 °C, IR $\nu_{\max}/\text{cm}^{-1}$ = 3103 (C-H), 2897 (C-O), 1607 (C=O), 1132 (OH), 934, 683, <sup>1</sup> H-NMR (500 MHz, D <sub>2</sub> O) $\delta_{\text{H}}$ 8.87 (s, 1H, ArH), 7.49 (s, 2H, ArH), 4.99-5.043 (m, 2H, CH), 1.74 (d, 6H, Me), <sup>13</sup> C-NMR (126 MHz, D <sub>2</sub> O) $\delta_{\text{C}}$ 174.9, 135.0, 121.67, 59.8, 17.37.
			C <sub>21</sub> H <sub>10</sub> N <sub>2</sub> O <sub>4</sub> (mol. wt. 364.39) M.P. 244 °C, IR $\nu_{\max}/\text{cm}^{-1}$ = 3023 (C-H), 1625 (C=O), 1293 (C=N), 845, 531, <sup>1</sup> H-NMR (500 MHz, DMSO) $\delta_{\text{H}}$ 9.37 (s, 1H, ArH), 7.50 (s, 2H, ArH), 7.17-7.18 (m, 6H, Ph), 6.98 (s, 4H, Ph), 5.27-5.30 (dd, 2H, CH), 3.48-3.51 (dd, 2H, CH <sub>2</sub> ), 3.19-3.24 (dd,

3.

2-(3-(1-carboxy-2-phenylethyl)-1H-imidazol-3-ium-1-yl)-3-phenylpropanoate (AIZ-3)



$^1\text{H}$ ,  $\text{CH}_2$ ),  $^{13}\text{C}$ -NMR (126 MHz, DMSO)  $\delta_{\text{C}}$  168.86, 136.61, 136.18, 128.67, 128.53, 126.85, 121.66, 64.43, 38.02.

**Table 2:** The weight loss parameters obtained for mild steel in 1 M HCl containing different concentrations of AIZs

Inhibitors	Conc (mM)	Weight loss (mg)	$C_R$ ( $\text{mg cm}^{-2} \text{h}^{-1}$ )	Surface Coverage ( $\theta$ )	IE (%)
<b>Blank</b>	0.0	230	7.67	---	---
<b>AIZ-1</b>	0.14	46	1.53	0.80	80.00
	0.27	37	1.23	0.84	83.91
	0.41	28	0.93	0.88	87.82
	0.55	23	0.77	0.90	90.00
<b>AIZ-2</b>	0.14	39	1.30	0.83	83.04
	0.27	23	0.77	0.90	91.00
	0.41	16	0.53	0.93	93.04
	0.55	15	0.50	0.93	93.47
<b>AIZ-3</b>	0.14	29	0.97	0.87	87.39
	0.27	20	0.67	0.91	91.30
	0.41	12	0.40	0.95	94.78
	0.55	09	0.30	0.96	96.08

**Table 3:** Values of  $E_a$ ,  $K_{\text{ads}}$  and  $\Delta G^0_{\text{ads}}$  at optimum concentration (0.55mM) of AIZs for mild steel in 1.0 M HCl at 308 K.

Inhibitors	$E_a$ (kJ mol <sup>-1</sup> )	$K_{\text{ads}}$ (10 <sup>4</sup> M <sup>-1</sup> )	$\Delta G^0_{\text{ads}}$ (kJ mol <sup>-1</sup> )
<b>Blank</b>	28.48		

<b>AIZ-1</b>	81.33	3.39	-37.00
<b>AIZ-2</b>	89.43	4.17	-37.53
<b>AIZ-3</b>	101.64	4.35	-37.64

**Table 4:** Tafel polarization parameters for mild steel in 1 M HCl solution in absence and at different concentration of AIZs

<b>Inhibitors</b>	<b>Conc (mM)</b>	<b><math>E_{corr}</math> (mV/SCE)</b>	<b><math>\beta_a</math> (mV/dec)</b>	<b><math>-\beta_c</math> (mV/dec)</b>	<b><math>i_{corr}</math> (<math>\mu\text{A}/\text{cm}^2</math>)</b>	<b><math>IE</math> (%)</b>
<b>Blank</b>	---	-445	70.5	114.6	1150	----
<b>AIZ-1</b>	0.14	-538	98.9	133.8	246.0	78.60
	0.27	-520	61.0	98.1	215.0	81.03
	0.41	-534	91.4	156.8	153.0	86.69
	0.55	-543	88.5	124.5	132.0	88.52
<b>AIZ-2</b>	0.14	-533	110.6	165.9	245.0	78.69
	0.27	-543	95.6	164.8	179.0	84.43
	0.41	-537	115.5	162.8	143.0	87.56
	0.55	-522	61.9	93.2	121.0	89.48
<b>AIZ-3</b>	0.14	-541	109.0	155.9	225.0	80.43
	0.27	-542	156.7	157.0	159.0	86.17
	0.41	-529	73.3	143.2	126.0	89.04
	0.55	-526	78.1	117.0	95.0	91.73

**Table 5:** EIS parameters obtained for mild steel in 1 M HCl in absence and presence of different concentration of AIZs

<b>Inhibitors</b>	<b>Conc (mM)</b>	<b><math>R_s</math> (<math>\Omega</math>)</b>	<b><math>R_p</math> (<math>\Omega</math> cm<sup>2</sup>)</b>	<b><math>n</math></b>	<b><math>C_{dl}</math> (<math>\mu F</math> cm<sup>-2</sup>)</b>	<b><math>IE</math> (%)</b>
<b>Blank</b>	---	1.12	10.7	0.83	106.21	----
<b>AIZ-1</b>	0.14	1.01	49.0	0.83	102.66	78.16
	0.27	0.67	82.9	0.76	100.64	87.09
	0.41	0.66	105.7	0.74	96.63	89.88
	0.55	0.64	144.4	0.71	76.20	92.59
<b>AIZ-2</b>	0.14	0.51	69.9	0.86	64.56	84.69
	0.27	0.62	114.2	0.86	34.99	90.63

	0.41	0.45	155.6	0.87	32.15	93.12
	0.55	0.77	171.9	0.88	29.52	93.77
<b>AIZ-3</b>	0.14	0.78	84.7	0.86	105.12	87.36
	0.27	0.85	126.0	0.87	63.83	91.50
	0.41	1.02	149.2	0.88	54.92	92.82
	0.55	0.80	204.4	0.89	98.21	94.76

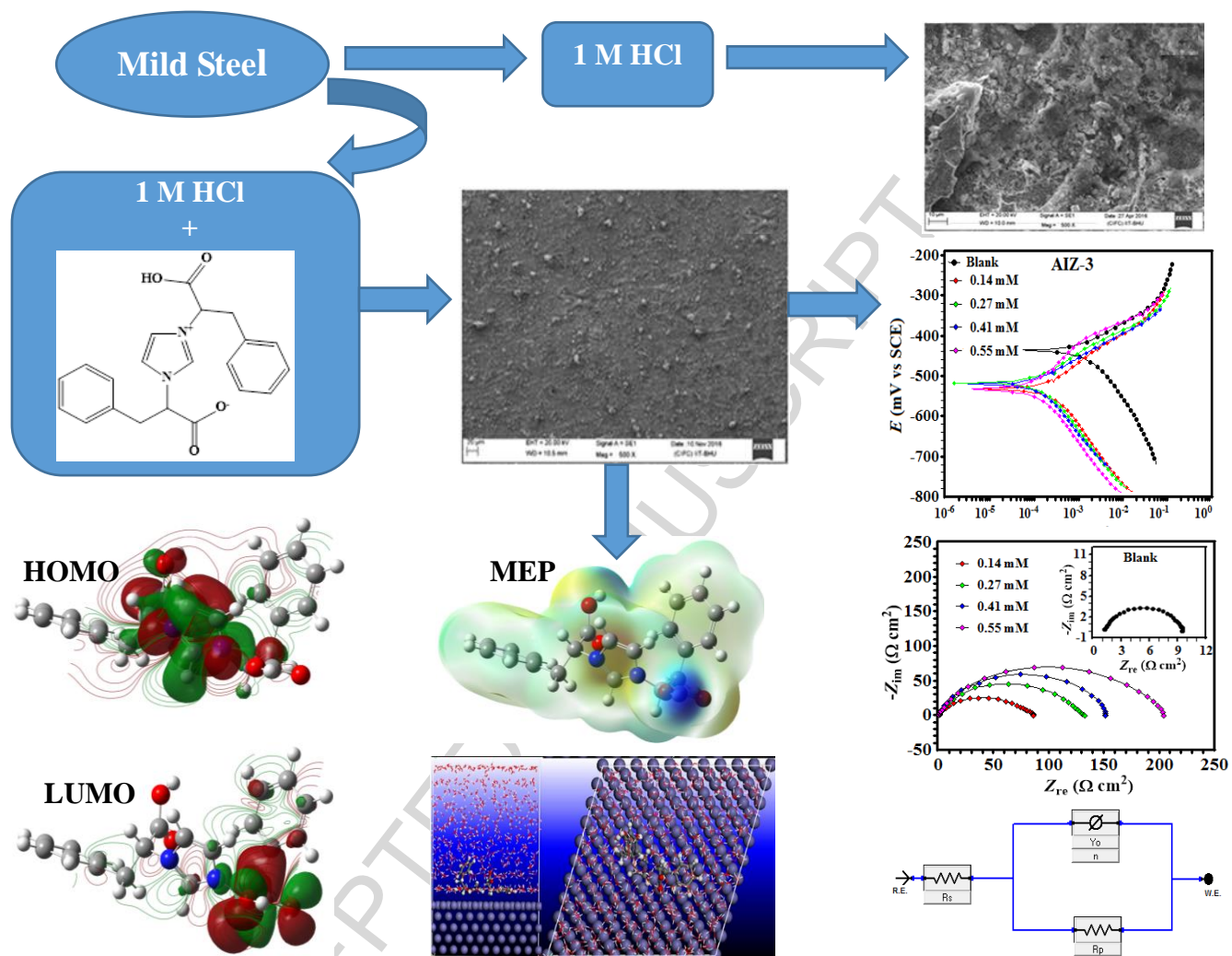
**Table 6:** Quantum chemical parameters of protonated form of AIZs inhibitor derived from the B3LYP/6-311G(d,p) method in aqueous phase

Parameters→	$E_{\text{HOMO}}$	$E_{\text{LUMO}}$	$\Delta E$	$\eta$	$\sigma$	$\chi$	$\Delta N_{110}$	$\omega$	$\varepsilon$
Inhibitors↓	(eV)	(eV)	(eV)	(eV)	(eV)	(eV)			
<b>AIZ-1</b>	-2.86	-0.63	2.24	1.12	0.89	1.74	1.38	0.68	1.47
<b>AIZ-2</b>	-2.92	-0.69	2.23	1.12	0.90	1.80	1.35	0.73	1.37
<b>AIZ-3</b>	-2.92	-0.81	2.11	1.05	0.95	1.86	1.40	0.82	1.22

**Table 7.** Selected energy parameters obtained from MD simulations for adsorption of inhibitors on Fe (110) surface

<b>System</b>	<b><math>E_{\text{Interaction}}</math> (kJ/mol)</b>	<b><math>E_{\text{Binding}}</math> (kJ/mol)</b>
<b>Fe + AIZ-1 + 491H<sub>2</sub>O + 9H<sub>3</sub>O<sup>+</sup> + 9Cl<sup>-</sup></b>	-476.04	476.04
<b>Fe + AIZ-2 + 491H<sub>2</sub>O + 9H<sub>3</sub>O<sup>+</sup> + 9Cl<sup>-</sup></b>	-501.39	501.39
<b>Fe + AIZ-3 + 491H<sub>2</sub>O + 9H<sub>3</sub>O<sup>+</sup> + 9Cl<sup>-</sup></b>	-688.54	688.54

## Graphical Abstract



**Research Highlights**

1. Synthesized inhibitors (AIZs) act as efficient inhibitors for mild steel corrosion in 1 M HCl.
2. Maximum inhibition efficiency of AIZ-3 was obtained at 0.55 mM.
3. Adsorption of AIZs obeys the Langmuir adsorption isotherm.
4. AIZ-1 act as cathodic inhibitor while AIZ-2 and AIZ-3 show mixed type behaviour.
5. Experimental results were supported by QC calculation and MD simulations.

ACCEPTED MANUSCRIPT